# Linear and Nonlinear Optical Study of Multilayer Ferroelectric Polymer Systems

By

Jennifer Jones

Dissertation
Submitted to the Faculty of the
Graduate School of Vanderbilt University
in partial fulfillment of the requirements
for the degree of

DOCTOR OF PHILOSOPHY

in
Interdisciplinary Materials Science

May, 2015

Nashville, Tennessee

Approved:

Dr. Norman Tolk

Dr. Kane Jennings

Dr. Jim Davidson

Dr. Deyu Li

Dr. Eva Harth

**To my wonderful children, Teagan and Glen, who helped me maintain my child-like enthusiasm**

**and**

**To my amazing husband, John, for his never-ending love, support and encouragement**

## ACKNOWLEDGEMENTS

First, I would like to give special thanks to my advisor Dr. Norman Tolk, not only for giving me the opportunity to perform research with the CMASS group but for providing me with professional and personal guidance. I would like to acknowledge my committee, Dr. Kane Jennings, Dr. Jimmy Davidson, Dr. Deyu Li, and Dr. Eva Harth for their helpful suggestions, comments and discussions.

There are several groups that were highly involved in my graduate career and I would like to thank the members of each. The past and current members of the CMASS group at Vanderbilt University; Dr. Halina Krzyzanowska, Dr. Stephanie Gilbert-Corder, Dr. Heungman Park, Dr. Travis Wade, Joy Garnett, Zina Jarrahi, and Andrey Baydin for their advice on classes, research and life in general. The friendships forged here will last a lifetime. Also, the past and current members of the NMSG group at Fisk University; Dr. Richard Mu, Dr. Eugene Collins, Dr. Roberto Aga, Daniel Mayo, and Anthony Mayo for their wisdom, support and enthusiasm. I also want to acknowledge the Fisk to Vanderbilt Bridge Program; Dr. Keivan Stassun, Dr. Arnold Burger, Dr. David Ernst and Dr. Dina Stroud for their support and guidance. Finally, the members of Platform IV of CLiPS at Case Western Reserve University; Dr. Lei Zhu, Dr. Eric Bear, Dr. Matt Mackey, Jung-Kai Tseng, and Joel Carr for their expertise on multilayer polymer films, and providing samples and XRD data.

Most importantly, this journey would not have been possible without the love and support of my family. I would like to thank my parents, whose words of wisdom and encouragement have guided me through many adventures. I would like to thank my brother and sisters. Their constant reminders of childhood kept me from taking myself too seriously. Thank you to my niece and

nephew, Madison and Evan, who taught me that no challenge is too big and superhero strength can come in little packages. Last but certainly not least, I wish to thank my husband, John, my daughter, Teagan, and my son, Glen. They are the motivation and inspiration for everything I accomplish.

Financial support for this project was provided by the NSF Science and Technology Center for Layered Polymeric Systems (CLiPS) (Grant 0423914) and ONR (W911NF-13-1-0153).

## TABLE OF CONTENTS

**Page**

## LIST OF TABLES

**Table** **Page**

## LIST OF FIGURES

# CHAPTER 1

# INTRODUCTION

## Introduction to dissertation

The experiments reported in this dissertation have led to further understanding of the ferroelectric properties of single and multilayer PVDF films, and will have significant impacts on the development of these films for electrical energy storage, such as capacitors, and piezoelectric applications. The work described involves the development of confocal Raman, second harmonic generation (SHG) and electric field induced second harmonic generation (EFISH) techniques to characterize novel multilayer poly(vinylidene fluoride)/polycarbonate (PVDF/PC) polymer films fabricated by co-extrusion technology.

This dissertation starts with a concise description of the most relevant and basic materials and technology as an introduction (Chapter 1). Then, extra care has been given in the following chapters to make them as self-contained and comprehensive as possible so that they can serve as independent chapters or papers. Thus, a brief outline of the dissertation may be summarized as follows:

In the further sections of this chapter (Chapter 1), the structure of the PVDF polymer is first described in detail. The structure and processing techniques that lead to its ferroelectric behavior are explained. A novel fabrication method developed by our collaborators at Case Western Reserve University (CWRU) called forced assembly via microlayer co-extrusion, and how it stands apart from other extrusion methods, is discussed. The final section of chapter 1

describes the theoretical consideration of SHG and the physical significance of the second order nonlinear susceptibility tensor, $\chi^{(2)}$.

Chapter 2 discusses the previous work of scientists that used PVDF polymers as second harmonic generators. One scientist, G. T. Boyd, motivated researchers to use SHG as a probe for studying the molecular ordering of poled polymers, and the research that followed is described. A comprehensive discussion of the work that CWRU has done with multilayer polymer films for capacitor applications identifies some of the challenges that can be addressed through the development of the confocal SHG and EFISH probe. Also, these films have a strong potential for applications as piezoelectric generators which has its own unique set of challenges that can also be served from these nonlinear optical techniques. The sections of this chapter motivate the research in this dissertation and provide a list of objectives specific to the challenges involved in developing these films for capacitor and piezoelectric applications.

Chapter 3 describes the development of the Ti:Sapphire laser and the preliminary work for the dissertation are discussed in detail. Two second harmonic experimental setups are described, both employing a Coherent Mira 900 Ti:Sapphire laser. A reflection SHG experimental setup is described and is used to compare SHG intensities from single layer PVDF films of different crystalline phase. The SHG intensities of multilayer PVDF-TFE/PET films that have β-phase crystalline domains of different orientations are compared. A second configuration in which SHG signals are measured in transmission is also developed. The addition of an EFISH testing platform and confocal SHG/EFISH configuration to the transmission setup are discussed.

Chapter 4 discusses the development of SHG as a probe for changes in crystalline domain orientation, molecular orientation and phase transitions as a function of temperature. This work

helped to further our understanding of the relaxation dynamics, β- and $\alpha_c$- relaxation, which occur in and effect the stability of the ferroelectric phase PVDF polymer films.

In chapter 5 the development of SHG as confocal probe for multilayer PVDF/PC films is examined. The SHG intensities of single layer extruded films of PVDF and PC are compared to that of 8 layer and 32 layer 50/50 PVDF/PC co-extruded films. These SHG measurements are then compared to confocal raman, FTIR, and XRD spectra. This work establishes a method for using the polarization of the fundamental laser beam and the orientation of the sample to identify the different polymer layers, and also provides important information about the interfaces between the polymer layers. This lays the groundwork for the further development of confocal SHG and EFISH laser spectroscopies.

In order to perform EFISH measurements transparent conducting electrodes must be deposited onto the surfaces of the films. A very commonly used transparent electrode material, ITO, tends to be brittle, which can be challenging when deposited onto a flexible polymer substrate. Chapter 6 involves experiments that help determine the best electrode material for EFISH measurements on PVDF/PC films by comparing UV-Vis absorbance spectra and resistivity of different materials at varying thicknesses. This is an important step for future EFISH measurements.

Chapter 7 describes the future work needed to completely develop confocal raman, SHG, and EFISH laser spectroscopies into a probe for multilayer PVDF/PC systems. Establishing and optimizing the resolution of these techniques, as well as understanding the dynamics of these systems with and without the application of an electric field are discussed.

The work described in this dissertation is important for the development of SHG and EFISH confocal laser spectroscopy, and can provide important information on electric field

distribution, structural changes, ion migration and the dielectric breakdown of PC/PVDF multilayer systems. This research can contribute significantly to the field for advanced energy storage and piezoelectric applications, and the results and fundamental understanding of the materials system will provide valuable guidance for better design principles of polymer multilayer films.

**Polyvinylidene Fluoride (PVDF)**

Polyvinylidene fluoride (PVDF) is truly a distinctive polymer due to the variation of crystalline phases it conforms to, and it has been extensively studied since Kawai discovered its strong piezoelectric response in 1969. The morphology of the polymer is highly process dependent and Kawai found that through mechanically drawing and electrical poling the β-crystalline phase, which is responsible for the piezoelectric response, can be obtained. In this section the polyvinylidene fluoride (PVDF) polymer and the formation of its crystalline structures are discussed in detail.

The PVDF monomer is produced using hydrocarbons and fluorocarbons which, after polymerization, has a repeat formula of $(CH_2\text{-}CF_2)_n$. One important feature of this monomer is that the fluorine atom is not much larger than the hydrogen atom. Fluorine has a van der Waals radius of 1.35 Å which is comparable to the hydrogen atom that has a van der Waal radius of 1.2 Å. The PVDF polymer can easily undergo crystallization and because of the small size of the atoms they are not forced into shapes, such as a helical, that can compromise the polarization of the polymer. They also do not suffer from the configurational defects commonly seen in polymers. If the $–CH_2$ in the PVDF monomer is referred to as the "head" and the $–CF_2$ is the "tail", polymers without configurational defects have a regular head-to-tail sequence. Configurational defects include head-to-head and tail-to-tail combinations occurring throughout the polymer. The PVDF monomer is also chemically stable and the resulting polymer chains typically do not cross link. Another important feature to note is that fluorine forms highly polar bonds with carbon with a dipole moment of $\mu = 6.4 \times 10^{-0}$ coulomb-meter.

Polymers are usually produced in a melt or solution process during which the polymer chains have randomly coiled shapes. When cooled from the melt configurationally disordered

polymers are forced to retain this random order. Polymers free of these configurational defects, such as PVDF, can undergo crystallization and have regular chain conformations when cooled. Chain conformations are described by the rotation angle of the single bonds between the carbon atoms and the most favorable conformations are those that minimize the potential energy of the chain. There are two such rotation angles; in *trans* or *t* arrangement the carbon atoms are rotated 180° such that the fluorine and hydrogen atoms are on opposite sides of the carbon chain as displayed in figure 1.1 (a). In the *gauche*$^{\pm}$ or $g^{\pm}$ arrangement the substituents are at ± 60° angles as shown in figure 1.1 (b).

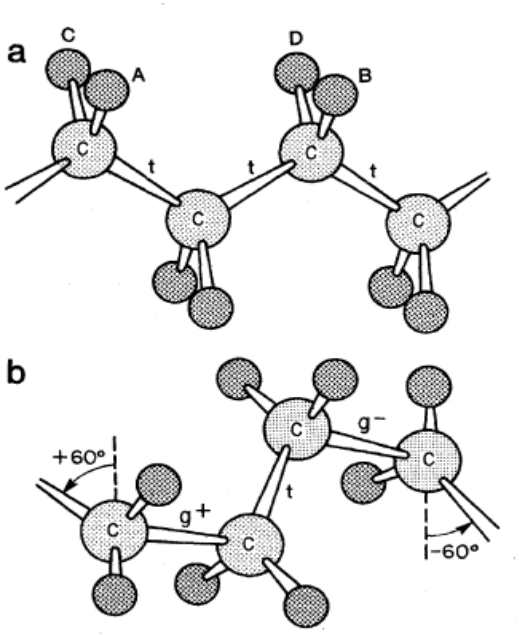


Figure 1.1: Schematic representation of polymer chain segments in different conformations: (a) *ttt* and (b) *tg+tg-*.[1]

PVDF has three known conformations which include the all-*trans*, $tg^{+}tg^{-}$, and $tttg^{+}tttg^{-}$. The most common of the three are the all-*trans* and the $tg^{+}tg^{-}$ and these are depicted in figure 1.2.

The all-*trans* chain conformation has dipole moments that are all in the same direction normal to the chain axis ($\mu = 7.0 \times 10^{-30}$ Cm). There is a polar moment in the $tg^+tg^-$ conformation and due to the inclination of the dipoles to the chain axis there are moments perpendicular to ($\mu = 4.0 \times 10^{-30}$ Cm) and parallel to ($\mu = 3.4 \times 10^{-30}$ Cm) the chain.

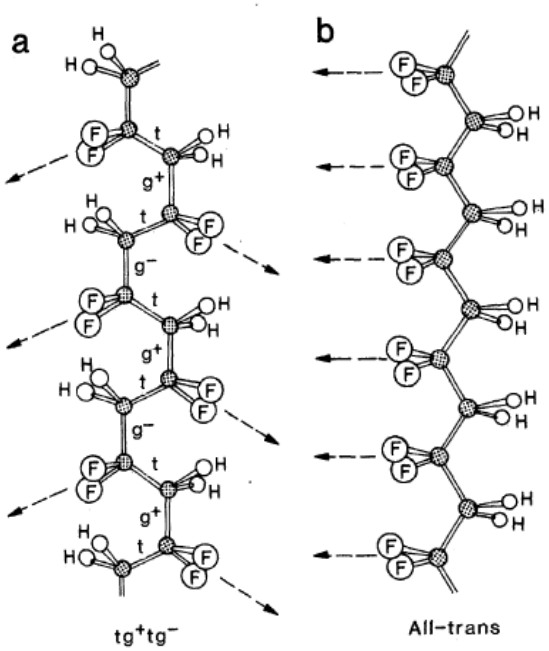


Figure 1.2: Schematic description of the two common crystalline phases of PVDF: (a) $tg^+tg^-$ and (b) all *trans*. The arrows indicate the dipole moments.[1]

Although PVDF has chain conformations that have strong polar moments when the polymer undergoes crystallization the chains can be crystallographically packed into a lattice so as to cancel each other's moments out. When cooled from the melt the most common crystalline phase for PVDF is the α-phase. The α-phase of PVDF suffers from such a cancellation as can be seen in figure 1.3 (a). The unit cell of this crystalline phase consists of two polymer chains of $tg^+tg^-$ conformation in which the polar moments perpendicular to the chain axis are oriented in opposite directions resulting in a net cancellation of polarization. The highly polarized crystalline

phase of PVDF is called the β-phase and is shown in figure 1.3 (b). The unit cell of a β-PVDF crystal consists of two chains with the all-*trans* conformation. The packing of this crystal structure results in the fluorine atoms of one chain being located at approximately the same level parallel to the *a*- axis as the hydrogen atoms in the neighboring chain. This arrangement is crucial in stabilizing the β-PVDF because of the preferred potential energy in this phase. However, as can be seen from figure 1.3, polymer crystals are extremely small.

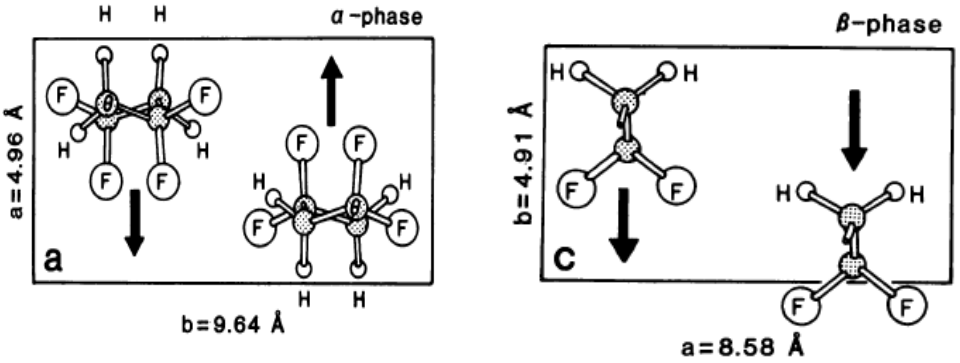


Figure 1.3: Unit cells of (a) α-phase and (b) β-phase PVDF shown in projection parallel to the chain axis. Arrows indicate dipole direction.[1]

When grown from the melt the PVDF crystals are arranged into spherical polycrystalline aggregates called spherulites that have no net polarization. The spherulites are a result of nucleation of primary crystals in the melt followed by radial growth outward from these nuclei in spherical envelopes.[1] Figure 1.4 (a) shows a typical image of spherulites of PVDF crystallized from the melt at 160°C as seen in a polarizing microscope. In this microstructure what appear to be radial fibers are actually stacks of very thin, platelet-like crystals called lamellae that are usually 10 nm thick and can be micrometers in length. The lamellae contain polymer chains that are crystallographically packed. Outside of the lamellae are polymer chains of unordered

conformations that define an amorphous region. These two phase structures are common in crystalline polymers and in PVDF approximately 50% of the polymer is crystalline lamellae and the rest is amorphous. When cooled from the melt PVDF crystallizes in the form of spherulites of the nonpolar α-phase.[1]

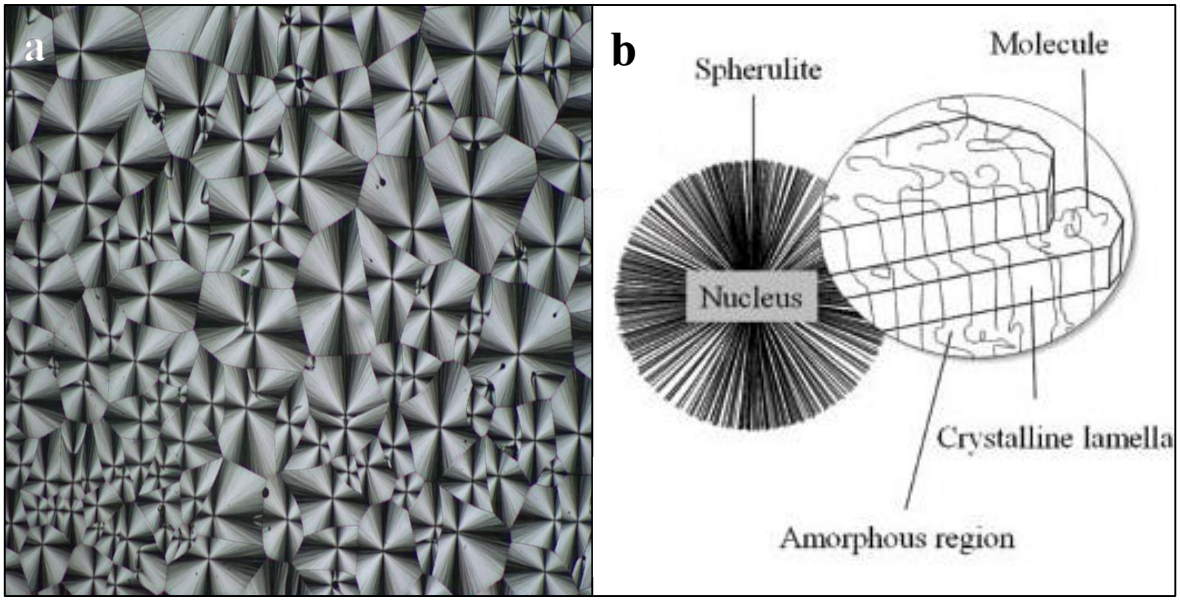


Figure 1.4: (a) Spherulites as seen from polarizing microscope. (b) Schematic representation of spherulites structure.

Because it requires high pressures or epitaxial techniques the β-phase of PVDF is not usually produced from the melt. To acquire β-phase PVDF conventional techniques involve mechanical stretching and electrical poling. This process can be seen in the schematic depicted in figure 1.5. The purpose of the mechanical stretching is to break down the spherulites formed during crystallization. This breakdown results in an array of crystallites whose polymer chains are oriented in the direction of the force. The temperature at which this process takes place is an important parameter. If the PVDF is stretched at temperatures near the melting point around 140° to 150°C the original $tg^+tg^-$ chains simply slide past each other. The result is a film that consists

of the crystals of the nonpolar α-phase. When the PVDF is stretched at temperatures below 90°C the polymer is less fluid and the polymer chains are forced into their most extended conformation which is the all-*trans* phase. The result is a PVDF film that consists of crystals of the highly polar β-phase with their chain axis oriented in the same direction. However, although their chains are in the same direction, the dipole moments of the individual chains are not uniformly oriented but point in random directions normal to the chains which can lead to a net cancellation of polarization. The next step in order to obtain a macroscopically polar film of PVDF is to apply an external electric field normal to the surface of the film. This will result in the alignment of the dipole moments of the polymer chains. The mechanism behind the field induced dipole reorientation of the β-phase PVDF is due to the psuedohexagonal (there is only about a %1 difference from hexagonal) packing arrangement of the chains in the unit cell. This suggests that when ferroelectric switching takes place in β-PVDF it does so in 60° increments.[2] The film is then slowly cooled while still under the application of the external electric field. This process essentially freezes the dipoles in place and the result is a ferroelectric thin film of PVDF.

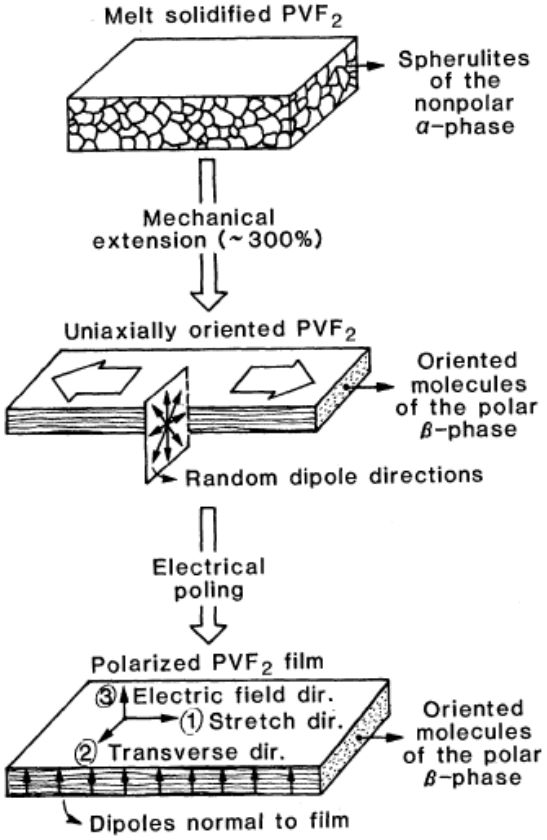


Figure 1.5: Schematic representation of the procedure employed to produce piezoelectric thin films of PVDF.[1]

**PVDF Co-Polymers:**

Polyvinylidene fluoride – trifluoroethylene (PVDF-TrFE) and polyvinylidene fluoride – tetrafluoroethylene (PVDF-TFE) are co-polymers that demonstrate similar ferroelectric behavior to PVDF. These co-polymers contain a greater portion of the heavier fluoride atoms than PVDF and as a result the molecular chains cannot accommodate the $tg^{+}tg^{-}$ chain conformation. Therefore, the molecular chains conform to the all-*trans* arrangement and crystallize into the β-phase when fabricated from the melt.[3] However, post processing techniques such as the mechanical stretching and electric poling as described earlier in the section are still necessary in order to orient the dipoles and render the film piezoelectric.

## An Overview of Multilayer Co-extrusion Enabling Technology

Large area, low cost production is a necessity if multilayer polymeric systems are to be successfully integrated into current technology. There is a production method already established for the fabrication of polymer thin films known as extrusion. An enabling technology developed by the Center of Layered Polymeric Systems (CLiPS) at Case Western Reserve University (CWRU) produces multilayered polymeric systems by using an advanced co-extrusion method. Describing these fabrication techniques in detail is the purpose of this section.

### *Extrusion*

Extrusion is a fabrication method that is capable of high volume manufacturing of polymer thin films. In this process raw polymeric materials are melted and formed into a continuous profile. The raw polymer material is in the form of small beads called resin. The resin is poured into a funnel like chamber called a hopper which is mounted onto and feeds the resin into the horizontal barrel of the extruder. The resin enters the feed throat of the barrel which is located at the rear of the barrel. It is then driven through the barrel by a rotating screw which forces the resin forward. Along the length of the barrel is a temperature gradient in which the temperature increases as the polymer travels further forward. The temperature from the back of to the front of the barrel is increased to the desired melt temperature of the molten polymer. This desired temperature is a parameter that is dependent on the type of polymer and is regulated using thermocouples. Temperature control is very important because there is a risk of degradation of the polymer if it is melted too fast.

At the front of the barrel, where the molten polymer leaves the screw, is a breaker plate that is supporting a screen pack that the polymer must travel through. The function of the screen pack is to remove any contaminates from the polymer. The breaker plate and screen pack also create a back pressure that in necessary for uniform melting and mixing of the polymer. This breaker plate/screen pack assembly also serves the purpose of converting the rotational memory of the polymer into longitudinal memory.

Once the molten polymer passes through the screen pack it then enters and passes through the exit die after which it is cooled in water. The exit die is what provides the final product its profile and there are many different types of exit dies that control the shape and thickness of the extruded polymer.

*Co-extrusion*

Co-extrusion is a type of extrusion process in which multiple extruders deliver a steady volumetric throughput of different molten polymers through a single exit die. This results in the extrusion of multiple layers of material simultaneously. In conventional co-extrusion techniques the thickness of the layers are controlled by the relative speeds and sizes of the individual extruders delivering the polymers.

*Forced Assembly via Microlayer Co-extrusion*

Microlayer co-extrusion is an advanced co-extrusion process that enables the production of layered films with anywhere from 2 to 4096 layers and film thicknesses ranging from 0.5mm to

1$\mu$m. It differs from the conventional multilayer co-extrusion in that many more layers, usually more than 50 but sometimes as many as several thousand are produced in one extrusion step. Two or three polymers can be incorporated in various arrangements; the most common are ABABAB… and ABCBABCB… Total thickness as well as layer thickness can be controlled, and in the case of thin films, the individual layer thickness may be reduced to a few tens of nanometers.[4,5]

This process is made possible by layer multiplying units with flow channels that cut, spread and recombine the melt to effectively double the number of incoming layers (figure 1.6). For a two component system, the number of layers is related to the number of multiplier units by *Number of Layers* = $2^{n+1}$ where $n$ is the number of multipliers.[4]

As the layer thickness approaches the micro and nanometer scale, useful and interesting mechanical[5], optical[6,7] and transport property[8] changes occur. For example, in dielectric applications the layered structure affects material morphology and electric field distributions which can improve or modify the dielectric properties of PVDF.[9] Thin films produced by microlayer co-extrusion exhibit interface regions that can also have an important impact on the material properties. In the case of nanolayered films, the interface thickness can approach the scale of the individual nanolayers, hence, creating a new material that is entirely interface.[10]

Understanding the mechanical, optical and transport properties of the materials in a multilayered polymer system as well as at the interfaces is crucial if polymers are to be integrated effectively into modern technology.

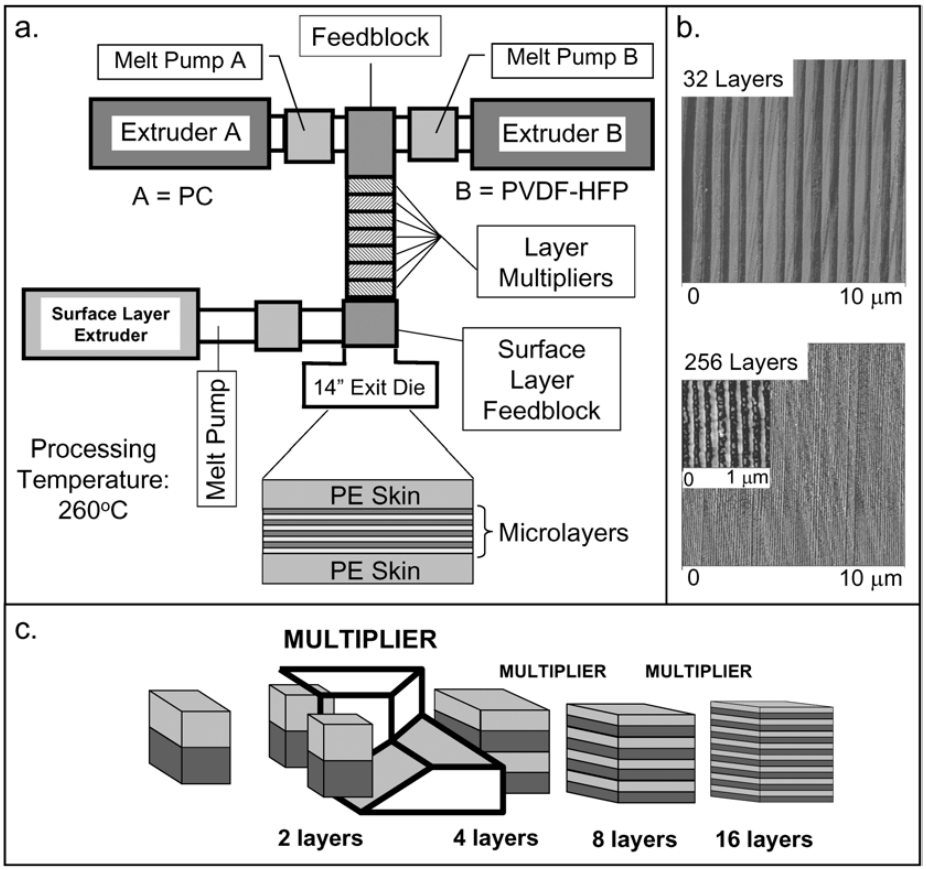


Figure 1.6: (a) Microlayer co-extrusion system. (b) AFM micrographs of 12 $\mu$m, 50PC/50PVDF-HFP films. (c) Schematic of multiplier flow channels.

## Second Harmonic Generation Laser Spectroscopy

Second harmonic generation (SHG) is described as the simplest of nonlinear optical processes. Of the 32 crystal classes only 21 are noncentrosymmetric and consequently can possess non-zero second-order susceptibility ($\chi^{(2)}$) which gives rise to the SHG signal. Applying a more restrictive condition that these crystals possess a permanent dipole moment gives rise to ferroelectric crystals, such as β-phase PVDF. The fact that an electric field in a material can greatly enhance SHG signals can be employed in a process known as electric-field-induced second harmonic (EFISH).

Previous work has shown that Second Harmonic Generation (SHG) laser spectroscopy can be used as a nondestructive, *in situ* and noninvasive probing tool that is very sensitive to characteristics of interfaces, making the technique well suited to layered material structures.[11-13] This research involves the development of SHG into a nondestructive probe for multilayer films in order to obtain information about the PVDF structure, phases, orientation and crystallinity in addition to interfacial properties of multilayered systems. In this section SHG is defined, the theory of SHG is explored and the physical significance of the second-order non-linear susceptibility to the generation of second harmonic light is discussed.

### *Theoretical Consideration of SHG*

Under normal conditions it is standard to treat the propagation of light classically; that is, there is a linear relationship between the electromagnetic field and the medium. Normal conditions being traditional light sources. The invention of the laser in the early 1960's was soon followed

by the discovery of nonlinear optics. The laser light is sufficiently intense enough to change the optical response of a medium from linear to nonlinear. Nonlinear optical phenomena are "nonlinear" in the sense that they occur when the response of a material system to an applied optical field depends in a nonlinear manner upon the strength of the optical field.[14] One example of nonlinear optics is second harmonic generation (SHG), which was first observed by Franken *et al.* in 1961. Second harmonic generation is the result of the part of the atomic response that depends quadratically on the strength of the applied optical field. This means that the intensity of the light generated at the second harmonic frequency tends to increase as the square of the intensity of the applied laser light.

To achieve a better understanding of optical nonlinearity, one needs to evaluate the response of a material's polarization $\vec{P}(t)$ to the strength of the applied electrical field $\vec{E}(t)$. In the classical case the strength of the optical field is quite small and results in a linear response where the electric polarization is in parallel with and directly proportional to the applied field. This relationship can be described by

$$\vec{P}(t) = \chi^{(1)}\vec{E}(t) \qquad (1.1)$$

where $\chi^{(1)}$ is the linear electric susceptibility and is a second rank tensor. When the condition is satisfied to use nonlinear optical treatment, the nonlinear optical response can be described by expressing the polarization $\vec{P}(t)$ as a Taylor expansion in a power series of the field strength $\vec{E}(t)$,

$$\vec{P}(t) = \chi^{(1)}\vec{E}(t) + \chi^{(2)}\vec{E}^2(t) + \chi^{(3)}\vec{E}^3(t) + \cdots \qquad (1.2)$$

$$\vec{P}(t) = \vec{P}^{(1)}(t) + \vec{P}^{(2)}(t) + \vec{P}^{(3)}(t) + \cdots \qquad (1.3)$$

where $\chi^{(2)}$ is the second-order nonlinear susceptibility and $\chi^{(3)}$ is the third-order nonlinear susceptibility. Also, $\vec{P}^{(2)} = \chi^{(2)}\vec{E}^2(t)$ is the second-order nonlinear polarization and $\vec{P}^{(3)} = \chi^{(3)}\vec{E}^3(t)$ is the third-order nonlinear polarization.

The simplest nonlinear optical process is that of second harmonic generation, which is illustrated schematically in figure 1.7. In the first illustration a laser beam with frequency ω impinges upon a crystal which has nonzero second-order susceptibility $\chi^{(2)}$ and a beam with a frequency of 2ω is generated. The second illustration describes second harmonic generation in terms of quantum mechanics where two photons with a frequency ω and energy ħω are absorbed and a photon with frequency 2ω and energy 2ħω is created simultaneously in a single quantum-mechanical process. The solid horizontal line is representative of the ground state and the dashed lines are representative of virtual states.

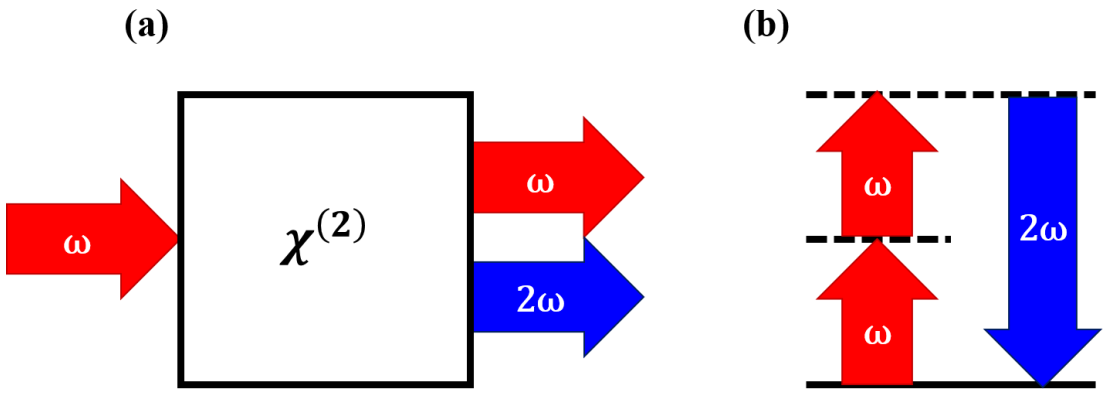


Figure 1.7: (a) Geometry of second harmonic generation. (b) Energy-level diagram describing second harmonic generation

In the classical model used to describe the linear optical response, when light is interacts with a material the lattice vibration may be treated as a simple harmonic oscillator. The lattice

oscillates within a potential well with a restoring force that obeys Hooke's law, and the potential energy curve is approximately harmonic. When the incident beam is sufficiently large however, the strong interaction will lead to the nonlinear response and the restoring force no longer increases linearly with the displacement. With this violation of Hooke's law the potential energy curve deviates from the parabola. The difference in form of this deviated energy curve from a parabola depends on the molecular/lattice structure of the material. Molecular structures can be described as noncentrosymmetric (without a center of symmetry) and centrosymmetric (with a center of symmetry). The potential energies for each can be seen in figure 1.8 where second harmonic generation can be expressed in terms of the nonlinear polarization oscillating at a frequency of $2\omega$.[14]

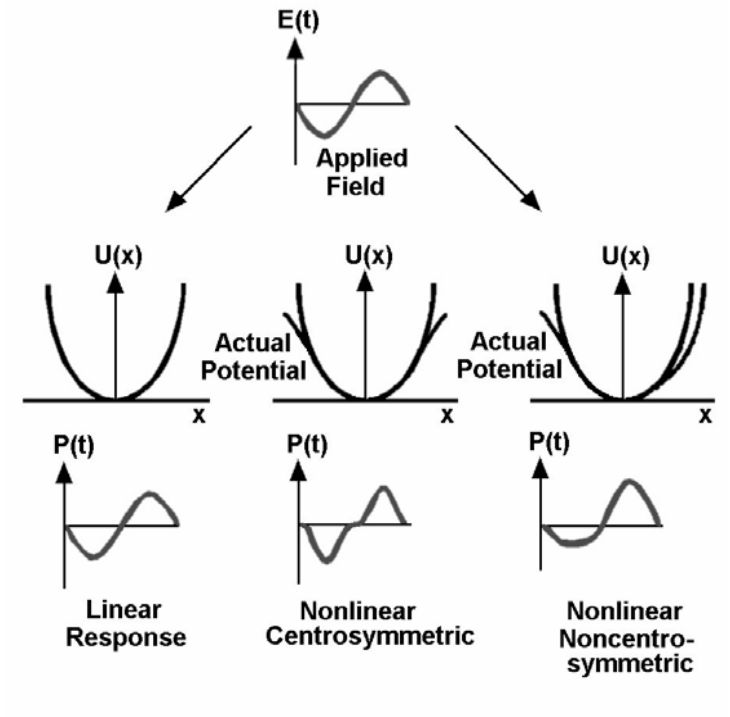


Figure 1.8: Correlation between the applied field *E(t)*, the potential energy *U(x)* and the polarization *P(t)* for centrosymmetric and noncentrosymmetric materials.

As stated previously, when the incident beam is sufficiently large the interaction of the beam with the material is nonlinear and the polarization depends on the electric field strength. The electric field strength can be described as

$$\vec{E}(t) = Ee^{-i\omega t} + c.c. \quad (1.4)$$

The second order nonlinear polarization that is generated in the crystal can be given as

$$\vec{P}^{(2)} = \chi^{(2)}\vec{E}^2(t) = 2\chi^{(2)}EE^* + \left(\chi^{(2)}E^2e^{-2i\omega t} + c.c.\right) \quad (1.5)$$

The first term shows the contribution of the zero frequency to the second order nonlinear polarization, and the second term shows the contribution from the doubled frequency 2ω. The zero frequency contribution is responsible for a process known as optical rectification where there is a generation of a static electric field within the nonlinear crystal. The contribution from the second term is clearly the generation of the radiation at the second harmonic frequency. This is responsible for the conversion of the output of a laser to different optical regions.

*Physical Significance of* $\chi^{(2)}$

The second order non-linear optical susceptibility is an inherent material property described by $\chi_{ijk}^{(2)}$, a third rank tensor. In the case of second harmonic generation the components of the second-order susceptibility tensor are proportionality constants that relate the amplitude of the second-order polarization to the product of electric field amplitude. The index *i* refers to the component of the second harmonic field, and indices *j, k* refer to the Cartesian components of the fundamental field. In the classical case all the indices are real and obey the anharmonic oscillator. The imaginary part of the nonlinear susceptibility is determined by the absorption coefficient of

the material. Through symmetry the nonlinear polarization leading to second-harmonic generation can be described in terms of the second-order susceptibility tensor by the matrix equation.[14]

$$\begin{bmatrix} P_x(2\omega) \\ P_y(2\omega) \\ P_z(2\omega) \end{bmatrix} = \begin{bmatrix} \chi^{(2)}_{xxx} & \chi^{(2)}_{xyy} & \chi^{(2)}_{xzz} & \chi^{(2)}_{xxy} & \chi^{(2)}_{xxz} & \chi^{(2)}_{xyz} \\ \chi^{(2)}_{yxx} & \chi^{(2)}_{yyy} & \chi^{(2)}_{yzz} & \chi^{(2)}_{yxy} & \chi^{(2)}_{yxz} & \chi^{(2)}_{yyz} \\ \chi^{(2)}_{zxx} & \chi^{(2)}_{zyy} & \chi^{(2)}_{zzz} & \chi^{(2)}_{zxy} & \chi^{(2)}_{zxz} & \chi^{(2)}_{zyz} \end{bmatrix} \begin{bmatrix} E_x E_x \\ E_y E_y \\ E_z E_z \\ 2E_x E_y \\ 2E_x E_z \\ 2E_y E_z \end{bmatrix} \quad (1.6)$$

Similar conditions that apply to crystal structures in on order to generate a second harmonic response also apply to ferroelectric behavior. Materials with a noncentrosymmetric crystal structure and permanent polarization exhibit ferroelectric behavior. Interestingly, the symmetry requirements for both phenomena (SHG and ferroelectricity) are identical, as both are described mathematically by the same third rank tensor, $\chi^{(2)}_{ijk}$. Ferroelectric β-phase PVDF thin films have the same symmetry property as the mm2 crystal class of the orthorhombic system.[13] For this crystal class the nonlinear polarization leading to second harmonic generation can be written as

$$\begin{bmatrix} P_x(2\omega) \\ P_y(2\omega) \\ P_z(2\omega) \end{bmatrix} = \begin{bmatrix} 0 & 0 & 0 & 0 & \chi^{(2)}_{xxz} & 0 \\ 0 & 0 & 0 & 0 & 0 & \chi^{(2)}_{yyz} \\ \chi^{(2)}_{zxx} & \chi^{(2)}_{zyy} & \chi^{(2)}_{zzz} & 0 & 0 & 0 \end{bmatrix} \begin{bmatrix} E_x E_x \\ E_y E_y \\ E_z E_z \\ 2E_x E_y \\ 2E_x E_z \\ 2E_y E_z \end{bmatrix} \quad (1.7)$$

If the incident beam is *p*-polarized, the x component of the optical field is zero and the nonlinear polarization becomes

$$\begin{bmatrix} P_x(2\omega) \\ P_y(2\omega) \\ P_z(2\omega) \end{bmatrix} = \begin{bmatrix} 0 & 0 & 0 & 0 & \chi^{(2)}_{xxz} & 0 \\ 0 & 0 & 0 & 0 & 0 & \chi^{(2)}_{yyz} \\ \chi^{(2)}_{zxx} & \chi^{(2)}_{zyy} & \chi^{(2)}_{zzz} & 0 & 0 & 0 \end{bmatrix} \begin{bmatrix} 0 \\ E_y E_y \\ E_z E_z \\ 0 \\ 0 \\ 2E_y E_z \end{bmatrix} = \begin{bmatrix} 0 \\ 2\chi^{(2)}_{yyz} E_y E_z \\ \chi^{(2)}_{zxx} E_y^2 + \chi^{(2)}_{zzz} E_y^2 \end{bmatrix} \quad (1.8)$$

Thus, it can be seen that if the incident beam is *p*-polarized light the second harmonic light generated from β-phase PVDF is also *p*-polarized with y and z components.

The SHG intensity can be described in terms of the second order nonlinear polarization:

$$I^{(2\omega)} = \left| P^{(2)}(2\omega) \right|^2 \quad (1.9)$$

After substituting equation 1.5 we get

$$I^{(2\omega)} = \left| \chi^{(2)} \right|^2 \left( I^{(\omega)} \right)^2 \quad (1.10)$$

From this equation it can be seen that the intensity of the second harmonic generation signal is quadratically dependent on the intensity of the incident fundamental beam, where the fundamental beam intensity is $I^{(\omega)} = E(\omega)E(\omega)$.

Of the 32 crystal classes only 21 are noncentrosymmetric and consequently can possess non-zero second-order susceptibility $\chi^{(2)}$which gives rise to the SHG signal. Applying a more restrictive condition that these crystals possess a permanent dipole moment gives rise to ferroelectric crystals. Ferroelectricity in a material can result in an electric field when there is an applied force or external pressure. The fact that an electric field in a material can greatly enhance SHG signals can be employed in a process known as electric-field-induced second harmonic (EFISH).

The intensity of the SHG signal can then be described by:

$$I^{(2\omega)}(t) = \left|\chi^{(2)} + \chi^{(3)}E_{dc}(t)\right|^2 \left(I^{(\omega)}\right)^2 \quad (1.11)$$

Where $I^{(\omega)}$ is the intensity of the incident laser beam, $E_{dc}$ is the varying time dependent electric field, and $\chi^{(2)}$and $\chi^{(3)}$ are the second- and third- order electrical susceptibilities.

SHG can be associated with very local environments at the nanometer scale. Therefore, the study of the physics of SHG can provide a wealth of information to understand the material properties down to the nanoscale. It is a very powerful tool to investigate material interfaces with both SHG and EFISH, which is why the research in this dissertation involves the study of polymeric single layer and multilayered systems. Further, since the PVDF and its copolymers only possess ferroelectric properties in a highly oriented β-crystalline phase, SHG can also be great *in-situ* diagnosis tool for β-phase formation and phase transition, and many other physical processes which may be difficult to analyze, such as relaxation dynamics.

# CHAPTER II

# BACKGROUND

## Literature review of SHG on PVDF

Soon after the discovery of the laser in 1960 [18] the phenomenon of SHG was demonstrated by Franken et.al. using a pulsed ruby laser and a quartz crystal.[19] In 1969 Kawai, a Japanese scientist, discovered that PVDF films become highly piezoelectric by mechanically stretching and electrically poling.[20] In 1970 J. G. Bergman *et. al.* were the first group to study the pyroelectricity and second harmonic generation from stretched and electrically poled PVDF films. Classifying highly oriented PVDF films as ferroelectric, they concluded that PVDF films can be used as pyroelectric sensors as well as a material to serve as a frequency-doubler from a neodymium laser as effectively as a lithium niobate crystal.[21] These observations prompted a large number of investigations of the piezoelectricity and pyroelectricity of PVDF. It wasn't until 1977 that R. G. Kepler and R. A. Anderson reported the use of diffracted Cu $K\alpha$ x-rays the intensity to demonstrate that the electrical poling process orients the crystalline axes of the thin films of PVDF, hence confirming that PVDF is, in fact, ferroelectric.[22]

Ten years later, in 1987, G. T. Boyd suggested that SHG can be used to characterize the molecular non-linearity and ordering in electrically poled materials. Using PVDF he illustrated that SHG can be used to determine the chain and C-F bond ordering. He also used SHG to study the dynamics of bond rotation during the poling process. Boyd concluded:

> Measurement of the $\chi^{(2)}$elements of poled polymer films can be used to determine the orientational parameters of the molecular bonds which are oriented by mechanical stretching and the application of an electric field. Optical SHG allows these measurements to be made during the application of the field, so that the ordering process may be directly observed. The formalism was applied to PVDF films to reveal the orientation of the polymer chains and the orientation of the C-F bonds about the poling direction.[23]

One of the challenges to produce ferroelectric PVDF films via mechanical stretching and electric poling is the limited degree of dipole and domain polarization ordering and relaxation room temperature. This relaxation could be the result of steric effects, dipole-dipole interactions and thermal randomization and relaxations in amorphous region as well. Boyd stated that static and dynamic studies of the dipolar orders are needed and that "a combined effort of many diagnostic tools (including SHG), as well as a concerted materials effort, will be necessary to optimize poled polymer films for their ultimate use in electro-optical signal processing."[23]

Considerable efforts have been made to optimize the ferroelectric properties of poled PVDF polymer films by modifying and observing the effects of different post processing techniques over the years. SHG has been used as a diagnostic tool to optimize poled polymer films, such as PVDF. In fact, SHG measurements have been one of the most effective ways to demonstrate the level of molecular ordering achieved in their films.

Bauer *et. al.* investigated the effects of electric poling and the distribution of polarization in PVDF thin films by studying the intensity of the SHG signal as a function of incident angle.[24-26] Others studied the SHG intensities of PVDF film prepared under different conditions such as, vapor deposition[27] and Langmuir–Blodgett.[28] In order to further optimize PVDF films many

scientists turned to the fabrication of PVDF blends, co-polymer and nanocomposite systems, as well as PVDF nanofibers in order to achieve higher molecular ordering and better stability of the β-crystalline phase. Some of these scientists used SHG to probe the molecular ordering of these systems.[29-32]

To conclude, considerable SHG research on PVDF polymers has been done in the past and the most relevant research highlights have been summarized in this section. It is neither complete nor comprehensive. It becomes clear though that the SHG technique is a very sensitive and powerful tool to study ferroelectric polymers such as PVDF. However, the potential to bring SHG to a new level, to apply SHG on new systems in order to provide new, unique, and critical information still exists. As described in previous and upcoming sections, this development is what my research dissertation has been based on. This research combines linear and nonlinear laser spectroscopy, conventional and confocal techniques along with novel and enabling sample fabrication technology to 1) demonstrate that this powerful but simple laser spectroscopy has various basic and practical applications and 2) provide new knowledge and understanding to this highly functional PVDF polymer systems.

**Critical review on co-extruded PC/PVDF multilayer films for capacitor applications**

The literature review information presented in this section is exclusively related to PVDF and PC systems. This is a critical step to provide up-to-date information and knowledge to readers and establish the ground work for my dissertation. Some knowledge may be valid to other insulating polymeric systems but it is not general enough to translate to other materials without careful evaluation.

There are five types of polarization in dielectric materials, namely, electronic ($P_e$), atomic ($P_{at}$), (dipolar) orientational ($P_{dip}$), ionic ($P_{ion}$), and interfacial ($P_{int}$) polarization.[33] These are shown in figure 2.1 in which the top panel shows the molar polarization (or the real part of permittivity) and the bottom panel shows the dissipation factor (or the imaginary part of permittivity).[33]

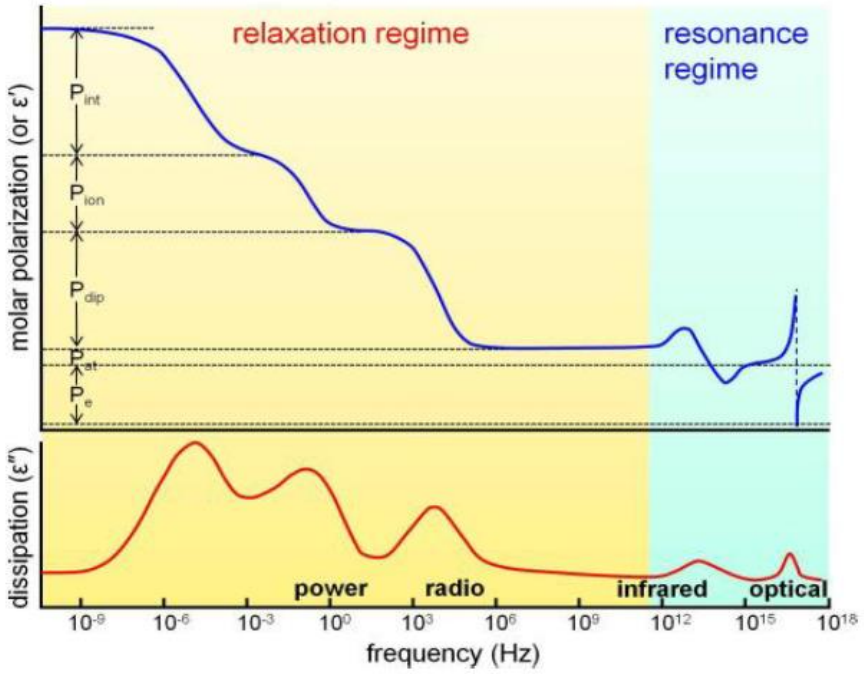


Figure 2.1: Different types of polarization as a function of frequency in polymers.[33]

In the case of polymer dielectrics, electronic and atomic polarizations are ubiquitous. These polarizations have no dielectric loss in the power and radio frequency application because their relaxation frequency is above THz. When a polymer contains permanent dipoles, such as the case of α- and β-phase PVDF, the dipolar orientation polarization takes place. This polarization occurs between 10 Hz and a few MHz depending on the relaxation mode, local environments, and temperature. Ionic polarization occurs when the polymer contains ions. This type of polarization takes place in the sub-Hz frequencies due to the slow migration of ions. Finally, the interfacial polarization, often referred as *Maxell-Wagner-Sillars* (MWS) interfacial polarization,[35] takes place at low frequencies. MWS interfacial polarization is the least understood regardless of its importance in many practical applications such as nanodielectrics, nanocomposite electrets, electro-magnetic shielding, and colloid-based electroheological fluids.[33] It can occur either at the interface between two polymeric dielectric materials, in the case of multilayer films, or at the electrode-sample interface (i.e., electrode polarization).

Co-extrusion multilayer polymer film fabrication technology can produce layer thicknesses ranging from micro- to nano-scales, as described in previous sections. This technology has resulted in several break-through inventions over the past decade, including enhanced mechanical properties, better packaging films for food, gradient refractive index (GRIN) lenses, polymer lasers, optical data storage, and advanced dielectric films.[33, 36-50] Multilayering of a high dielectric constant polymer [e.g., poly(vinylidene fluoride) (PVDF) and its copolymers] with a high dielectric breakdown polymer [e.g., polycarbonate (PC)] produced a high energy density and low loss dielectric film.[34, 47] This work led to a few patent application, thus laying the groundwork for using multilayer polymer films as dielectric capacitor films.[51]

*Understanding the energy loss in PC/PVDF multilayer films*

To achieve high energy density and low loss capacitors, the materials need to have high dielectric constant, high dielectric breakdown, and low losses. Demonstration of the nature of the capacitive energy loss is important and necessary. As shown in figure 2.2, charged, discharged energy densities, and energy loss can be easily obtained by the electric displacement electric field (D-E) loop tests.

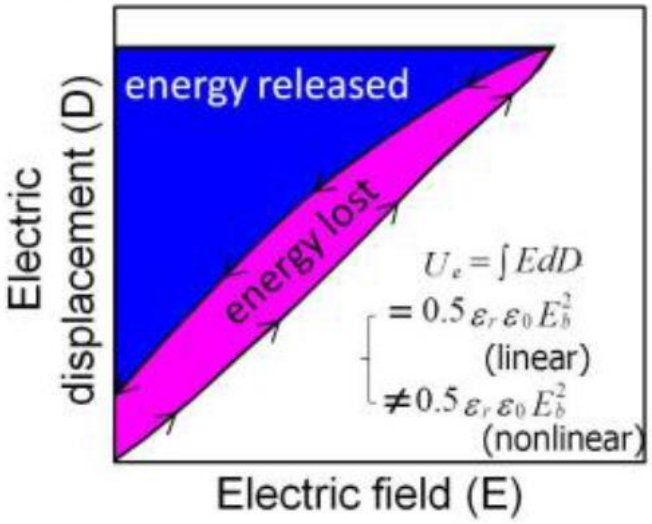


Figure 2.2: Charged, discharged energy densities, and energy loss in a D-E loop test.

Compared to ferroelectric PVDF which exhibits significant hysteresis in D-E loops, the PC/PVDF 50/50 multilayer films exhibit a reduced hysteresis as can be seen in figure 2.3 (a), (b), and (c). However, The group at CWRU has shown that the VDF dipoles do not switch in multilayer films when the PC content is above 50 vol% by performing a polarized electric field dependent FTIR study on uniaxially stretched PC/PVDF multilayer films.[36] It is suggested that the lack of dipolar switching *could be explained* by the non-uniform electric field distribution in

multilayer films. The electric field in the PVDF layer should only be ~1/4 that in the PC layer due to the difference in the dielectric constants. PC has a low dielectric constant of $\varepsilon_r = 2.8$, and PVDF has a high dielectric constant of $\varepsilon_r = 12$. The low nominal electric field in PVDF might not be strong enough to switch the VDF dipoles. The question still remains why is there hysteresis in the dielectric loop?

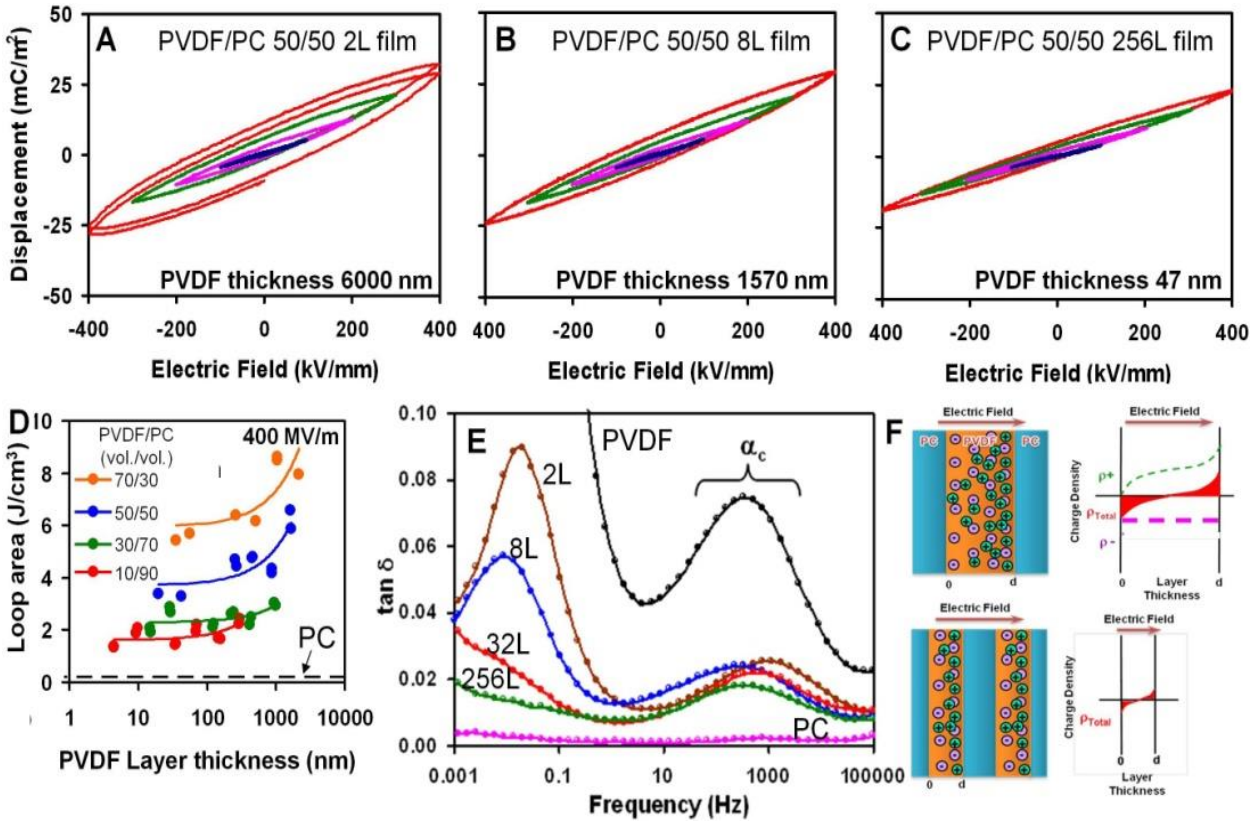


Figure 2.3: Attempt to explain energy loss in PC/PVDF multilayer films. The top panel shows hysteresis loops for PC/PVDF 50/50 (a) 2-, (b) 8-, and (c) 256- layer films with different PVDF layer thicknesses. (d) Loop area as a function of PVDF layer thickness for different PC/PVDF compositions. (e) Dissipation factor, tanδ, as a function of frequency for PC PVDF 50/50 films with different number of layers. (f) Schematic of explanation of confined impurity ion migration in nanolayers. The right side shows decreased ion migration in thin PVDF layers.[36]

Another observation CWRU made is that the area of the hysteresis loop decreases with decreasing PVDF layer thickness [see figures 2.3 (a) and 2.3 (d)].[36] This *can be explained* by the

confined impurity ion migration effect, shown in figure 4E & F. Impurity ions are extremely difficult to remove and exist in many brands of PVDF and its copolymers due to the suspension polymerization method. Even if the impurity ions are only present on a ppm-level, the result is that there is significant ion relaxation in polar polymers.[49] This can be seen in figure 4E where the dielectric loss in pure PVDF exhibits a significant low frequency ion migrational loss in addition to the famous $\alpha_c$ dipole relaxation at 500 Hz. However, by multilayering PVDF with PC and gradually decreasing the PVDF layer thickness (or increasing the number of layers), the low frequency ion migrational loss becomes negligible. In an attempt to explain the observation that the area of the hysteresis loop (energy loss) decreases with decreasing PVDF layer thickness, the illustration in figure 4F indicates that ion migration is significantly reduced under electric field when the PVDF layer thickness is reduced to nano-scales.

*Understanding the dielectric breakdown process in PC/PVDF multilayer films*

Another observation that CWRU made of PC/PVDF multilayer films is that the dielectric breakdown strength is 3 times enhanced as compared to a simple blend [figure 2.4 (b)] with simple layered structure. Efforts have been made to study the dielectric breakdown mechanisms through electrical testing, SEM and dual ion-beam SEM imaging. From optical and SEM imaging, they observed a treeing process at the polymer interfaces and attributed this mechanism to hampering charge penetration across the layers [see insets in figure 2.4 (b)].[34] For comparison purposes, the breakdown strength of 32-layer films of PC and polysulfone (PSF) were measured and it was found that the PC/PSF films do not exhibit any enhanced breakdown strength due to layering [figure 2.4 (a)]. This indicates the breakdown strength of multilayer polymer films is dependent on the

interface between two materials that have a large dielectric contrast. MWS interfacial polarization is thought to be induced at the PC/PVDF interfaces because of the difference in the dielectric constant (10-12 for PVDF vs. 2.8 for PC) and bulk conductivity (~$10^{-12}$ S/m for PVDF and ~$10^{-15}$ S/m for PC) for the two polymers, and the PC layer possibly serves as a blocking electrode [figure 2.4 (d)]. These interfaces can accumulate charges and can serve as effective charge traps, which explain the enhanced breakdown strength for multilayer films. However, it is determined that the thickness of the PC blocking electrode is also important. By performing a leakage current study, they saw that 32-layer films of PSF/PVDF 70/30 had a higher resistance than the 256-layer film [figure 2.4(c)]. It is determined that when the PC layer is very thin interfacial charges are able to tunnel through, as shown in the schematic on the right of figure 2.4 (d). There are two competing effects that are important to consider when optimizing the performance of the PC/PVDF multilayer films: 1) Mechanisms of ionic migration processes with PVDF layer thickness; 2) the roles of interface between PVDF and PC; And 3) the physics of why PC is an excellent charge blocking polymer and its effectiveness decreases when the layer thickness is very thin.

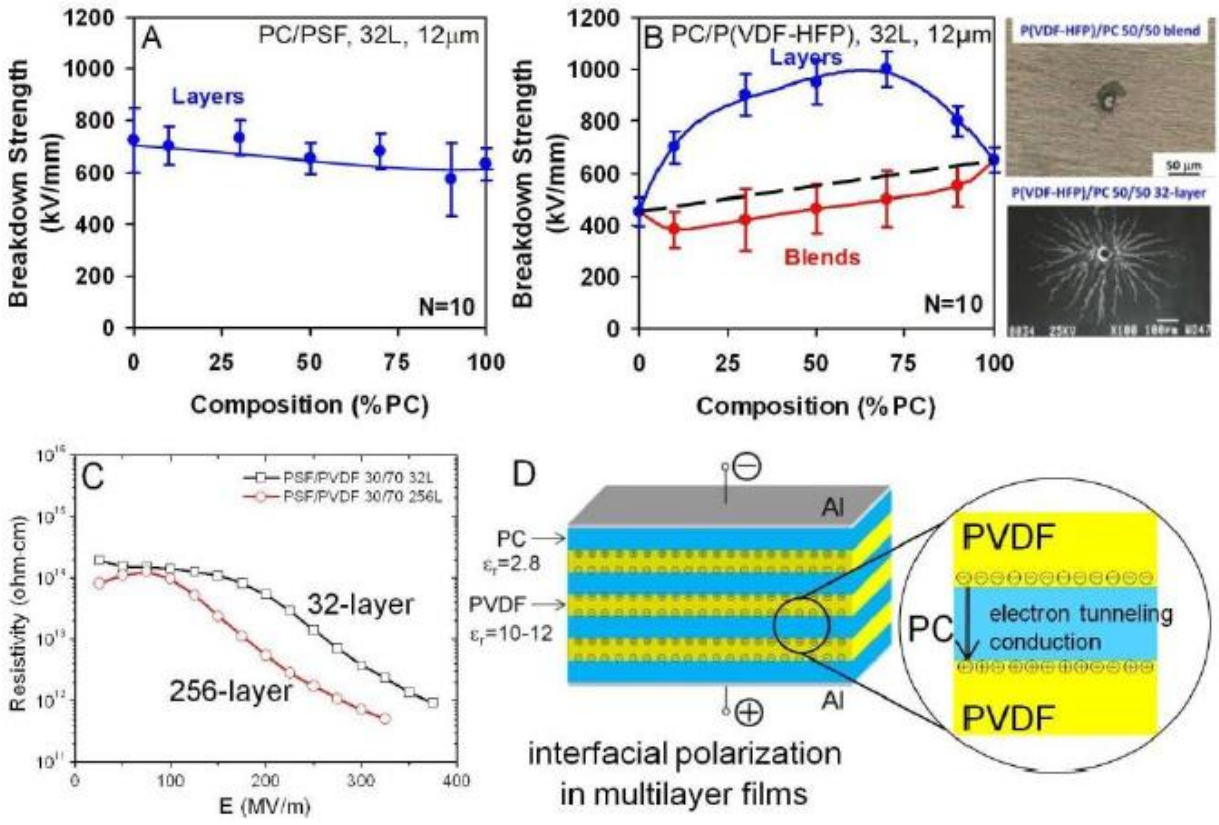


Figure 2.4: Dielectric breakdown strength as a function of PC composition for (a) PC/PSF and (b) PC/P(VDF-HFP) 32-layer films. Inset shows optical images of the breakdown holes for PC/P(VDF-HFP) blend and 50/50 32-layer film. (c) Resistivity as a function of electric field at room temperature. (d) Scheme of interfacial polarization in PC/PVDF multilayer films.

In conclusion, while multilayer films have shown promise for high energy density and low loss dielectric materials for capacitor applications, the understanding of the different types of polarizations in these systems is crucial for next steps in material optimization, development, and fabrication. The development of SHG and EFISH confocal laser spectroscopy can provide important information on electric field distribution, structural changes (dipolar orientation polarization), ion migration (ionic polarization) and the dielectric breakdown (MWS interfacial polarization) of PC/PVDF multilayer systems. It is, then quite obvious that this research can contribute significantly to the polymer dielectrics for advanced energy storage applications.

## Introduction to Research Objectives

Self-powering devices, sensors, and miniaturized systems via energy harvesting and storage from the environment presents a great opportunity in current and future technology. Current regenerative energy harvesting technology include photovoltaics, thermoelectric and kinetic approaches.[53,54] Piezoelectric-based devices for mechanical energy harvesting has drew considerable interests in recent years. Due to the very nature of ferroelectric materials, piezoelectric technologies can serve as both energy harvesting and energy storage devices, sensors, and systems.[55-57] Ferroelectric polymers, such as PVDF and its copolymers, have broad potential due to their flexibility, durability, low cost, light weight, non-toxicity, *etc*. Therefore, the study of piezoelectric properties of vinylidene fluoride based ferroelectric polymers in combination with multilayer co-extrusion enabling technology can bring high impact to breakthrough technology and scientific discovery.

Piezoelectric energy (PE) scavenging systems are arguably superior to two other types of regenerative energy generators; Faraday's Law based electromagnetic (EM) and capacitor based electrostatic transduction (CET). The advantages of piezoelectric electric generators include: 1) they are simpler in structure than EM and CET devices, 2) the direct conversion of vibrational energy into a voltage, 3) the ease of integration into macro-, micro- and nano-devices and systems; such as thin and thick films and multilayer integration with respect to EM devices, 4) they do not require an input voltage as oppose to CET systems, and 5) PE devices can deliver high voltage or high current depending on the fabricated device structure, as shown in figure 2.5. In addition, multilayered films also have a much higher dielectric breakdown strength than monolithic films and higher electric energy capacitive storage.[58]

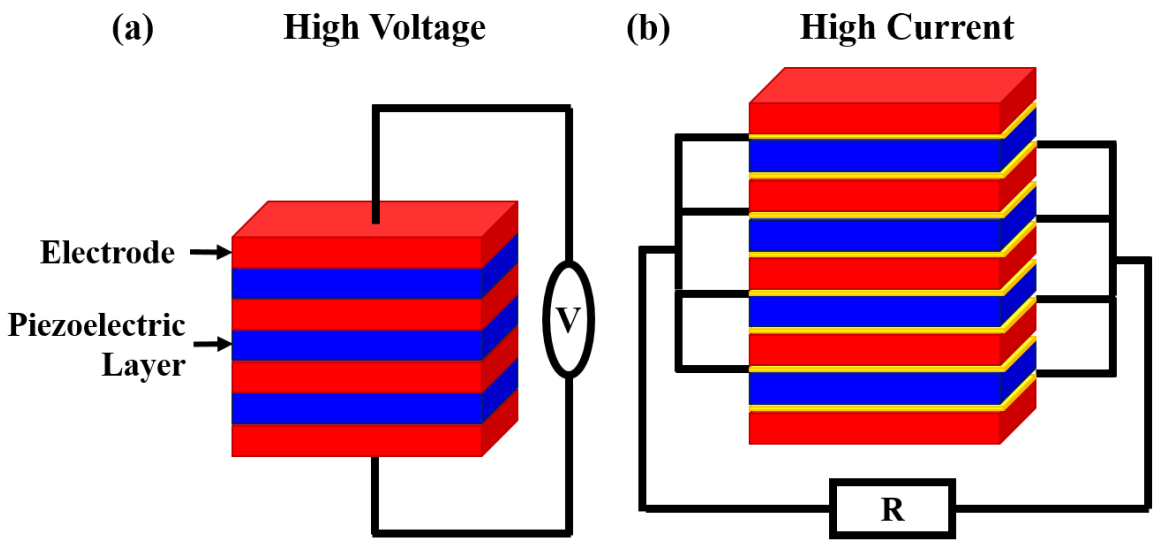


Figure 2.5: Schematic of piezoelectric generator for (a) high voltage and (b) high current.

Further, ferroelectric polymers, such as PVDF-TFE and PVDF-TrFE, are better candidates to achieve high quality β-phase and result in better piezoelectric effect.[59-61] However, there are a number of materials issues that require further piezoelectric effect study, which include; film thickness dependence, interfacial confinement effects on the stabilization of β-phase, impurities (such as, metallic ions or additive effects), as well as temperature dependence. Although the property evaluation mentioned above will not prevent the multilayer system development, it will directly affect technological breakthroughs both for energy harvesting devices and energy storage capacitors.

From a multilayer film capacitor aspect, as discussed in previous section, considerable research has been done by us and others. It has been demonstrated that dielectric breakdown strength can be dramatically enhanced by multilayering a high dielectric constant polymer with a high breakdown strength polymer.[62] Although it is speculated that the horizontal configuration of interfaces between two polymers plays an important role in enhancing the breakdown strength via

a treeing phenomenon no clear fundamental understanding has been provided/demonstrated thus far. The goal of this research is to examine and evaluate how important the interfacial polarization at the interface between two polymers is by developing a method to characterize the overall film, the individual layers, and interfaces between layers of a multilayer system. It is possible that the interfaces under appropriate conditions can serve as effective traps for real charges (i.e. electrons, holes and impurity ions). Therefore, direct electronic conductivity can be significantly reduced, and as a result, the breakdown strength will be enhanced.

Due to the fact that the co-extrusion technology is enabling and novel, this area of research is relatively open and much can be explored. From the materials characterization perspective, linear and non-linear confocal spectroscopy can address a number of important and critical issues which include: Second harmonic generation laser spectroscopy (SHG) to study PVDF films; confocal Raman spectroscopy to study PVDF containing multilayered dielectric films layer-by-layer with sub-micron spatial resolution; and SHG laser spectroscopy to investigate multilayer PVDF/PC co-extruded films from overall film measurements then venture into layer-by-layer. Also, the development of the confocal electric field induced second harmonic (EFISH) technique will allow mapping of the electric field inside the multilayer film when an external high voltage is applied. The results and fundamental understanding of the materials system will provide valuable guidance for better design principles of polymer multilayer films.

# CHAPTER III

# EXPERIMENTAL CONFIGURATION

## Introduction

In this chapter the development of the Ti:Sapphire laser and the preliminary work for the dissertation are discussed in detail. Two second harmonic experimental setups are described, both employing a Coherent Mira 900 Ti:Sapphire laser. A reflection SHG experimental setup is described and is used to compare SHG intensities from single layer PVDF films of different crystalline phase. The SHG intensities of multilayer PVDF-TFE/PET films that have β-phase crystalline domains of different orientations are compared. A second configuration in which SHG signals are measured in transmission is also developed. The addition of an EFISH testing platform and confocal SHG/EFISH configuration to the transmission setup are discussed.

## The Ti:Sapphire laser

Just four years after the development of the optical laser in 1960 the first tunable solid state laser, the Ni:$MgF_2$, was developed.[63,64] However, is wasn't until the tunable $Cr^{3+}$:$BeAl_2O_4$ laser, developed in 1979, was demonstrated to operate at room temperature that solid state lasers became more popular than the commonly used dye laser.[65-67] Twenty two years after the discovery of the laser, P. F. Moulton of MIT Lincoln Labs developed the Titanium-doped sapphire, or Ti:$Al_2O_3$,

laser. Today there are dozens of tunable solid state lasers, but none that have the tuning range of the Ti:Sapphire.

The working mechanism behind the spectroscopy of the Ti:$Al_2O_3$ crystal and its broad tuning range is the coupling between the of the electronic energy levels of the $Ti^{3+}$ ions to the phonons of the sapphire host crystal.[68] At room temperatures most atoms are in a lower energy state. A process referred to as pumping is required to raise the Ti atoms into their high energy or excited states for the light amplification to occur. In order to excite Titanium, each atom requires intense light, and therefore a Ti:Sapphire laser must be pumped by another laser. Sapphire is an ideal host crystal for the Ti:$Al_2O_3$ laser because it is transparent from the ultraviolet to the infrared, is very hard, and has excellent thermal conductivity. This combination of mechanical, thermal and optical properties of the Ti:$Al_2O_3$ crystal allow laser designs that result in high average powers.[68] The Ti:Sapphire laser used in the experiments reported in this dissertation is the Coherent Mira 900. The Mira 900 is pumped by a stable Coherent 10 W Verdi diode pumped 532 nm green laser and has a tunable wavelength range from 720 to 900 nm. There are several methods that exist in order to generate short, high powered pulses from Ti: $Al_2O_3$. Using a process known as self mode locking the Mira 900 produces 150 fs pulses at a repetition rate of 76 MHz and pulse energy of ~10 nJ.

## Sample preparation

### *Single layer piezoelectric commercial films*

To establish SHG as a sensitive, non-destructive, and *in-situ* characterization technique for industrially produced polymer thin films, commercially available films were purchased from Measurement Specialties, Inc. The PVDF films are produced from the melt via extrusion, uni-axially stretched to obtain the β-phase, and then electrically poled to orient the dipoles which results in a piezoelectric film. These films are mass produced and available to purchase in rolls by the foot. For these experiments samples are cut from a roll of 9 μm thick piezoelectric PVDF thin film. These samples are important for establishing SHG as a characterization technique because they have known polymer chain and dipole orientations.

### *Single and multilayer extruded films*

In order to establish SHG as a sensitive and non-destructive probe for characterizing multilayer polymer systems, single layer and multilayer films are fabricated by forced assembly via multilayer co-extrusion at Case Western Reserve University (CWRU).

Single layer films of PVDF and PC are extruded, and multilayer films of 2, 8 and 32 layers consisting of PVDF/PC 50/50 composition (by volume) are co-extruded. The films from this sample set have an overall thickness of 12 μm and no post processing manipulation is performed resulting in PVDF layers that consist of the α crystalline phase.

A second set of multilayer films consisting of co-polymer PVDF-TrFE/ Polyethylene terephthalate (PET) 50/50 composition are also fabricated by forced assembly via multilayer co-extrusion. Sample A is as-extruded while Sample B and C are bi-axially stretched at a draw ratio of 4.5 X 4.5 and Sample C is thermally treated at 120ºC. All samples (A, B, and C) have the β crystalline phase but the post processing manipulation of Samples B and C change the crystalline orientation from isotropic (Sample A) to on-edge and flat-on respectively. On-edge crystalline orientation refers to crystalline domains that have their polymer chains oriented parallel to the surface of the film. Flat-on crystalline orientation refers to the crystalline domains having polymer chains oriented perpendicular to the film surface.

Table 3.1: Description of the physical properties of PVDF-TFE/PET 50/50 multilayer samples A,B, and C

| **Sample A** | **Sample B** | **Sample C** |
|---|---|---|
| • Film thickness: ~ 10 µm<br>• Layer thickness: ~300 nm<br>• **No stretching**<br>• No thermal treatment<br>• No electric field poling<br>• Structure: PVDF-TFE is semicrystalline (**all β-phase**)<br>• Crystal orientation: **Isotropic**<br>• PET is amorphous | • Film thickness: ~ 10 µm<br>• Layer thickness: ~ 300 nm<br>• **Bi-axially stretched at 105ºC at draw ratio 4.5 X 4.5**<br>• No thermal treatment<br>• No electric field poling<br>• Structure: PVDF-TFE is semicrystalline (**all β-phase**)<br>• Crystal orientation: **on-edge**<br>• PET is amorphous | • Film thickness: ~ 9 µm<br>• Layer thickness: ~ 280 nm<br>• **Bi-axially stretched at 105ºC at draw ratio 4.5 X 4.5**<br>• Thermal treatment at 120ºC for 3 hours<br>• No electric field poling<br>• Structure: PVDF-TFE is semicrystalline (**all β-phase**)<br>• Crystal orientation: **flat-on**<br>• PET is amorphous |

**Introduction to preliminary work**

Non-centrosymmetric (NCS) PVDF and its co-polymers, when crystallized in β–phase, exhibit technologically important ferroelectric properties: piezoelectricity and pyroelectricity. It

is evident that piezoelectric PVDF polymer has distinct advantage over inorganic piezoelectric ceramic materials. It is flexible, light weight, optically transparent, cheap and easy to fabricate and can be produced in high volumes. However, its major drawbacks include partial crystal phase formation (50 – 70% crystalline phase), thermal stability, and relatively short lifetime of the ferroelectric form. With a multilayered system, it is possible to use particular polymer(s) as a confining layer to stabilize the confined PVDF layers and possibly maintain preferred crystalline phase and orientation. Therefore, it is believed that SHG and EFISH laser spectroscopy can serve as a powerful diagnosis tool to provide basic information in a non-destructive and in-situ manner. Certainly, the technology can be readily employed for other organic materials and device applications such as non-ferroelectric multilayer polymeric systems. In the following sections, some preliminary results are briefly summarized.

**Reflection SHG experimental configuration**

The simplest and most widely used method of measuring second harmonic generated signals is through the detection of the optical reflection of SHG. The majority of SHG experiments have an incident beam of frequency $\omega$ impinge on the surface of the material at an angle $\theta < 90°$ and the SHG beam of frequency $2\omega$ is generated in reflection.

A right angle reflection configuration of a SHG experimental set-up, shown in figure 3.1, is used to examine the feasibility and explore the potential applications of SHG and EFISH in layered polymeric systems with an emphasis on co-extruded multilayered films. In this configuration a sample set is placed on a silicon wafer at different positions vertically; because the films are transparent the Si acts as the reflecting surface. A red pass filter is prevents the 532 nm

light of the pump laser from reaching the sample. The 800 nm fundamental beam is incident on the sample at a 45° angle and is focused to a spot size of approximately 50 μm in diameter on the sample surface. The second harmonic generated beam is then separated from the fundamental beam using a blue pass filter, collected by a PMT and measured by a photon counter. The samples are mounted on a translation stage that changes the vertical position of the mounted sample set, hence changing the location of the incident fundamental beam. This allows direct comparison of the second harmonic intensity generated from the samples as well as the Si wafer. The sample mounting configuration is shown for each set of samples in figures 3.2 (a) and 3.3 (a).

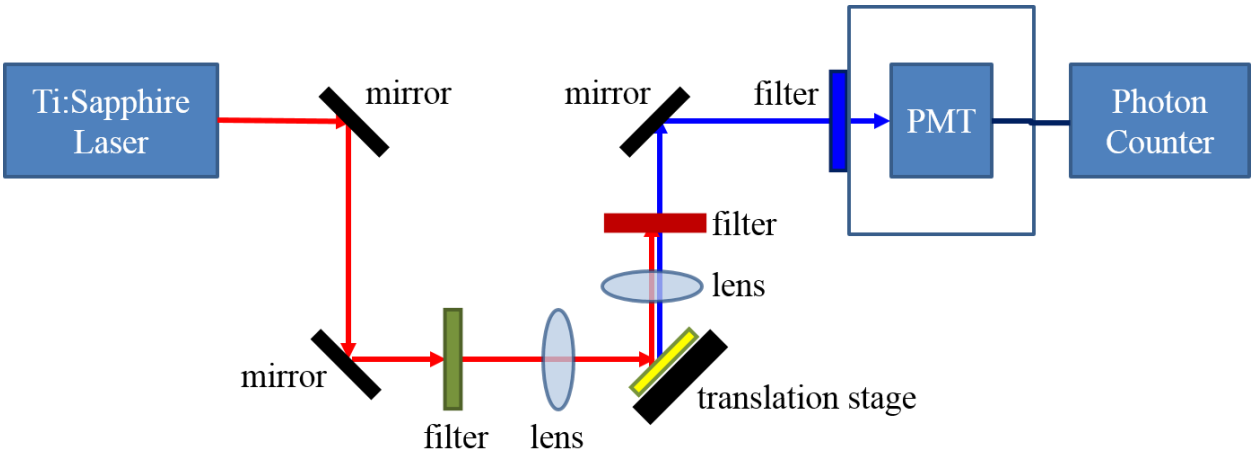


Figure 3.1: Schematic representation of a SHG reflection configured experiment

Two sets of materials systems are evaluated using the SHG reflection configuration described above: 10 μm single layer PVDF films and multilayered PVDF-TrFE/PET films of 10 μm thickness and 8 alternating repeats.

**Reflection SHG investigation of single layer PVDF films**

The SHG investigation of single layer PVDF films involves a direct comparison of the changes of second harmonic intensity generated by a commercial piezoelectric PVDF film produced at Measurement Specialties, Inc. and the extruded α-phase PVDF film fabricated at CWRU. Both films are mounted on a Si wafer, which serves as the reflecting surface. The films and Si wafer are then mounted on a translation stage that changes their position with respect to the focal spot of the incident fundamental beam as is represented in figure 3.2 (a).

The preliminary SHG results of the α-phase and piezoelectric (oriented β–phase) PVDF polymer films are shown in figure 3.2 (b). As the location of the incident beam is translated from impinging on the Si wafer to the α- PVDF film, the SHG intensity increases from ~200 counts (on Si wafer) to ~600 counts. A very sharp increase of SHG intensity to more than 400,000 counts is observed when the position of incidence is translated onto the piezoelectric (oriented β–phase) PVDF. In comparing the second harmonic intensities generated from these films it is clear that the highly oriented β-phase films result in a much stronger SHG signal than the α-phase films. This is due to the interaction between the strong optical field and the second order non-linear susceptibility ($\chi^{(2)}$) of the PVDF β-crystalline phase which is explained in detail in Chapter 1. These results demonstrate that SHG laser spectroscopy can be used to study the structure and physical properties of layered polymer films.

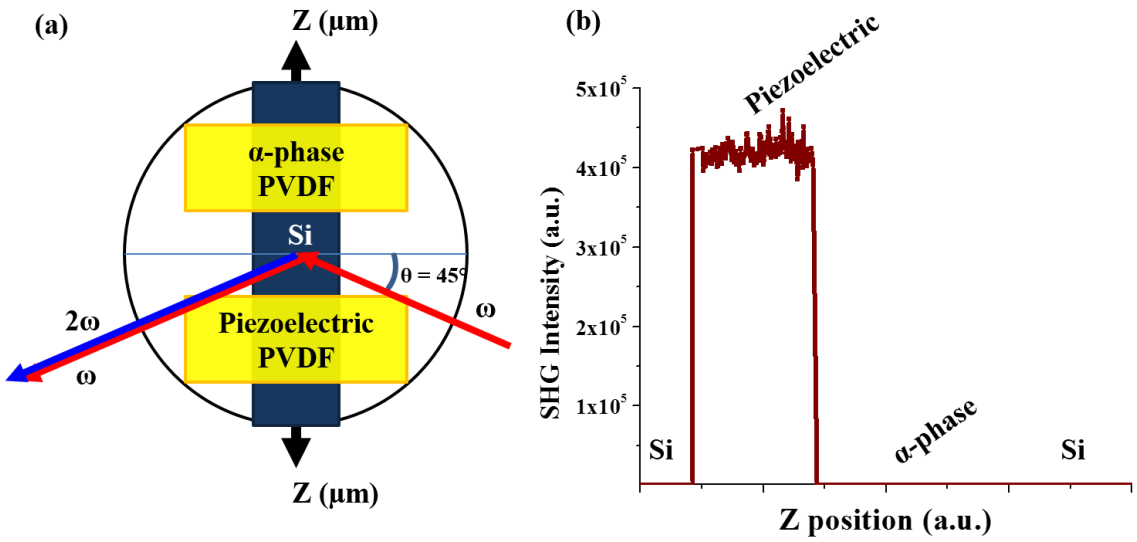


Figure 3.2: Comparison of second harmonic intensities generated by single layer α-phase and piezoelectric PVDF polymer films. a) Schematic of sample mounting and experimental configuration for reflection SHG. b) Reflected SHG signal of PVDF films and Si wafer.

**Reflection SHG investigation of PVDF-TFE/PET multilayered films**

The SHG investigation of the multilayer films involves a direct comparison of the changes of second harmonic intensities generated by three PVDF-TFE/PET multilayer films with different crystalline domain orientations as described in Table 3.1 (Samples A, B, and C). These films are fabricated by forced assembly via microlayer co-extrusion and provided by research collaborators, Profs. Baer and Zhu at CWRU. The experimental procedures used previously, using the translation stage to change the position of the samples with respect to the incident fundamental beam spot, are conducted on the multilayer samples and are shown in figure 3.3 (a). As can be seen in figure 3.3 (b) the second harmonic generated intensity from the Si wafer is at ~200 count. The SHG intensity of the sample with flat-on crystalline orientation is ~1100 counts. The samples with on-

edge and isotropic crystalline domain orientation have similar SHG intensities of around 400 counts.

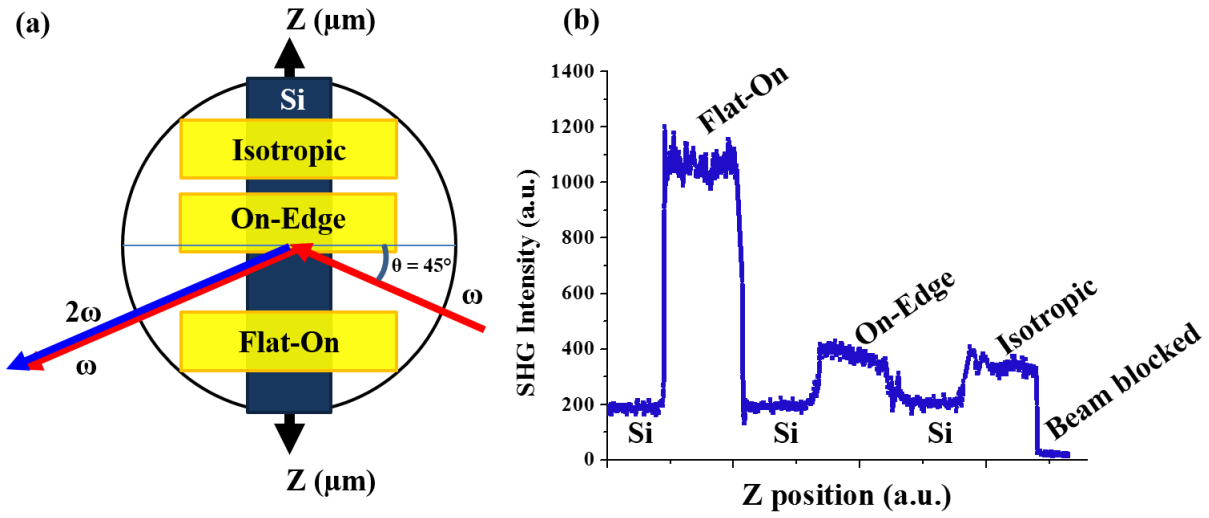


Figure 3.3: Comparison of second harmonic intensities generated by multilayer PVDF-TFE/PET polymer films with different crystalline orientations. a) Schematic of sample mounting and experimental configuration for reflection SHG. b) Reflected SHG signal of PVDF-TFE/PET multilayer films and Si wafer.

The known basic properties of these three samples are summarized in table 1. All three samples have approximately the same layer and total thicknesses. Sample A is as co-extruded, and although PVDF/TFE is in the β-phase the crystal domain orientation is random, resultig in a SHG signal that is reletively weak. Sample B is biaxially stretched at 105 $^{o}$C and the resulting SHG signal has no appreciable increase. A XRD study performed at CWRU shows that sample B's crystalline domains are edge-on, which defines the polarization of the aligned dipole moments as pointed along the film direction in 2-dimension. It is, thus, a signal average that is obtained. Clearly, sample C gives rise to a much stronger SHG intensity. The XRD shows that when the multlayered film was stretched and then thermally annealed at 120$^{o}$C, near its glass transition

temperature, for 3 hrs the crystal orientation becomes flat-on. Under this condition the polarization of β-phased piezoelectric crystal is along the film's surface normal, which in turn gives the strongest SHG signal. The results on multilayer PVDF-TFE/PET films indicate that the orientation of the β-phase crystalline domains greatly effects the intensity of the SHG signal.

Highly functional piezoelectric PVDF requires biaxial and uniaxial stretching, as well as electric poling to orient the dipoles and maximize its performance. Previous SHG studies have shown the strong dependence of the intensity of the SHG signal on the polarization of the incident beam and the crystal oritation as discussed in Chapter 2. The preliminary work here also indicates a strong relationship between the SHG intensity and the phase as well as the crystalline orientation of PVDF. Therefore, based on these facts, SHG can be used to provide a wealth of information about PVDF structure, phases, orientation, and crystallinity. Electric field induced second harmonic (EFISH) generation, on the other hand, can provide additional information on the physical properties of the interface and electric field distributions within multilayer polymer systems.

**Transmission SHG experimental configuration:**

Although the reflection SHG configuration is a simple and commonly used method of collecting a SHG measurement, the transparency of PVDF polymer films to the 800 nm fundamental and 400 nm second harmonic generated beams allows for a simpler configuration to be established. Figure 3.4 shows a schematic of a SHG experiment in which the fundamental beam impinges on the sample and the transmitted optical second harmonic signal is collected. This configuration has several advantages: the SHG signal from the Si wafer is removed from the

background, the distance the second harmonic beam travels through the sample is reduced, and there is a larger range of linear and angular translations available.

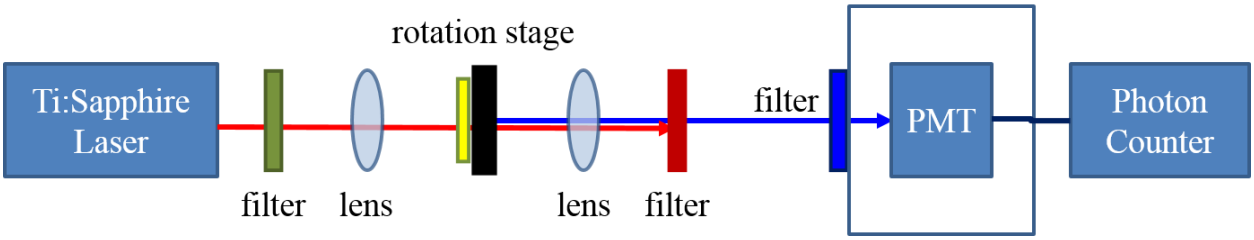


Figure 3.4: Schematic of transmission SHG experimental configuration.

Similar to the reflection configuration, the transmission experimental setup consists of a red pass filter that prevents the 532 nm light of the pump laser from reaching the sample. The angle of incidence of the 800 nm fundamental beam on the sample can be varied and is focused to a spot size of approximately 50 μm in diameter on the sample. The transmitted SHG beam is then separated from the fundamental beam using a blue pass filter, collected by a PMT and measured by a photon counter.

The samples are mounted in a computer controlled rotation stage that rotates the sample around the surface normal (azimuthal angle, $\phi$) during collection of the SHG signal. The first rotation stage is mounted on a second rotation stage giving precise control of the angle of incidence, $\theta$. This arrangement allows a direct observation of changes in SHG intensity with respect to the orientation of the sample which can provide important information on the structure of the PVDF films. The transmission SHG experimental setup is the basic configuration used for the experiments described in the following chapters of this dissertation.

**Electric field induced second harmonic generation (EFISH) experimental setup**

For EFISH measurements transparent conducting electrodes must first be deposited on the top and bottom surfaces of the polymer films. After electrode deposition the films will be tested with a dielectric testing platform equipped with a Keithley function generator providing the input signal and a precision high voltage generator from Trek which can produce voltages up to ± 4 KV. This testing platform will be combined with the transmission SHG experimental setup as shown in figure 3.5. With this arrangement information on the dielectric and structural properties of PVDF thin films and multilayer systems under the application of an external electric field can be obtained.

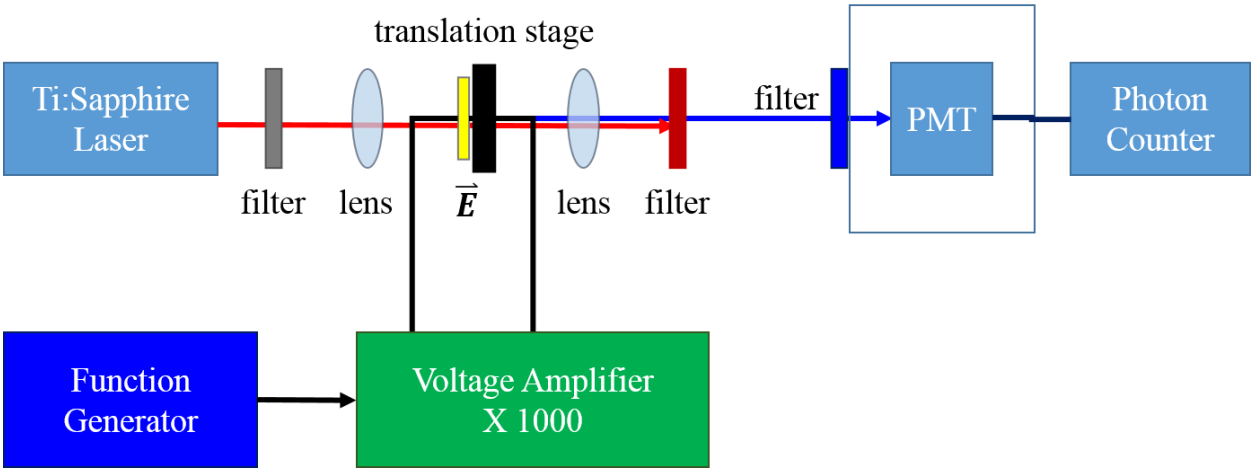


Figure 3.5: Schematic of EFISH experimental platform in combination with transmission SHG setup

**Confocal SHG**

The transmission SHG experimental configuration is very effective at collecting SHG signals from transparent polymer films. However, when collecting the SHG signal from multilayer polymer systems using this configuration it is a global view of the system that is measured. The SHG $\left(\chi^{(2)}\right)$ and EFISH $\left(\mathrm{E} * \chi^{(3)}\right)$ signals transmitted from every layer and every interface contribute, as can be seen in figure 3.6.

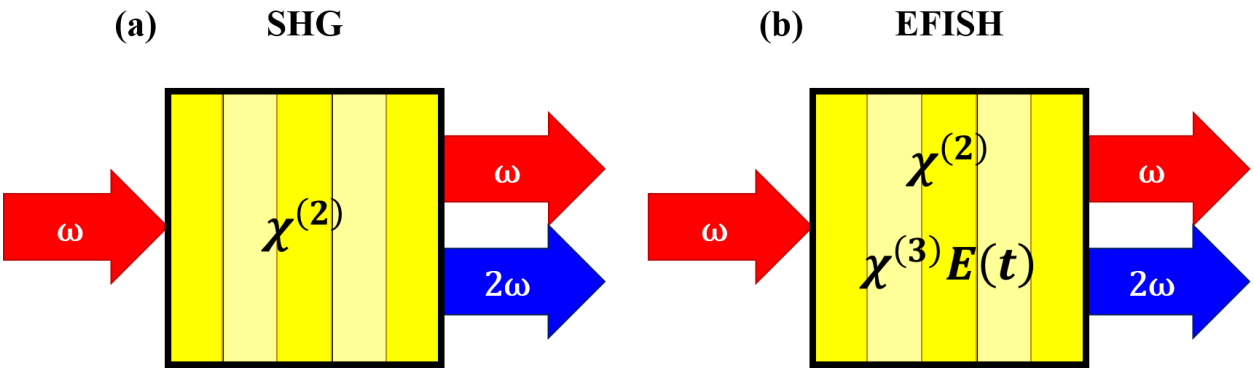


Figure 3.6: Transmission (a) SHG and (b) EFISH signals from multilayer polymer systems

The signals from entire multilayer system combine to give the final SHG signal that is detected by the PMT. This is an additive effect and is described using equation 3.1.

$$I^{(2\omega)}(t) = \sum_i \left|\chi_i^{(2)} + \chi_i^{(3)} E_i(t)\right|^2 \left(I^{(\omega)}\right)^2 \qquad (3.1)$$

However, this summation can lead to a very weak SHG signal, and does not provide specific information on the structure or properties of any single layer or interface. It is important to be able characterize the individual layers as well as the interfaces between layers in a non-destructive and *in-situ* manner. To do this a confocal SHG/EFISH setup must be established.

Confocal spectroscopy can provide excellent spatial resolution, and involves tightly focusing the fundamental beam, using a piezo stage to move the sample with respect to the focal point, and blocking signals from outside the focal point using a confocal aperture as illustrated in figure 3.7.

Confocal measurements will also be performed in the transmission mode. A 3D piezo-stage with two degrees of rotation will allow the study of SHG, EFISH, and Raman signals from individual layers and the interfaces between layers. With the addition of true confocal features and x-, y-, and z-piezoscan capability, 3D spectral mapping/imaging at diffraction-limited resolution is possible. The information obtained from the 3D submicron spectral mapping will provide critical, complimentary and supportive information to achieve the research objectives.

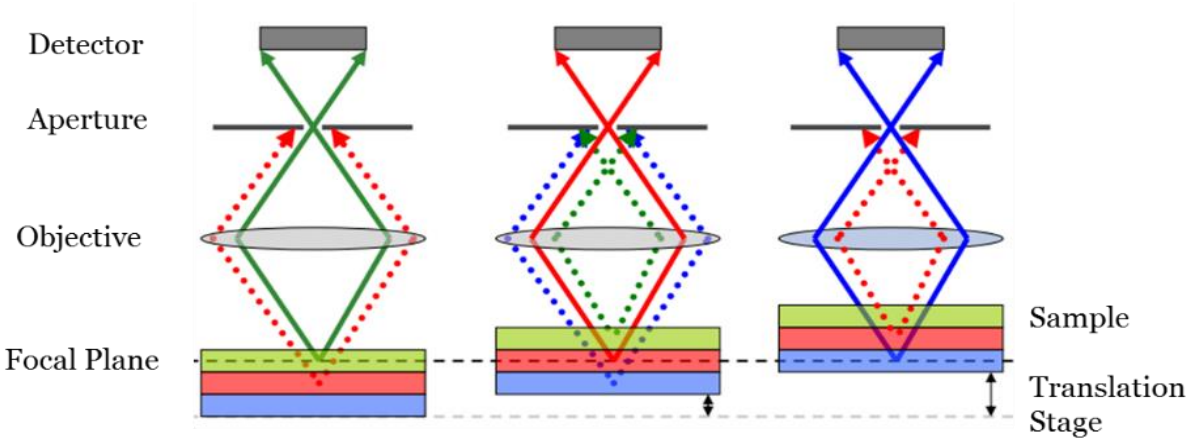


Figure 3.7: Schematic of confocal experimental configuration

**Summary**

In summary, the Ti:Sapphire laser and a reflection SHG experimental setup is described. The reflection SHG configuration is used to compare SHG intensities from commercial piezoelectric single layer PVDF film to an extruded α-phase film. This configuration is also used

to compare SHG intensities of multilayer PVDF-TFE/PET films that have β-phase crystalline domains of different orientations. It is concluded that SHG can be used to study physical structures such as crystalline phase and orientation of multilayer PVDF films. Finally, a transmission SHG experimental setup is described and this setup is used for the SHG measurements in the experiments that follow in this dissertation. Modifications to this setup that allow transmission EFISH and confocal SHG/EFISH measurements are also discussed.

# CHAPTER IV

# INVESTIGATION OF FERROELECTRIC PROPERTIES AND STRUCTURAL RELAXATION DYNAMICS OF PVDF THIN FILM VIA SECOND HARMONIC GERNERATION

## Introduction

Second harmonic generation (SHG) laser spectroscopy has been demonstrated to be a powerful, sensitive, and non-destructive analytical technique to study crystalline phases, domain and molecular dipole orientations, and relaxation dynamics of ferroelectric polymeric thin films of polyvinylidene fluoride (PVDF). While other spectroscopic techniques, such as WXRD and FTIR, do provide valuable information on crystalline phases, they are not sensitive enough to provide the detailed information at molecular levels and properties at interfaces. The current study of single layered PVDF polymer has shown that SHG can be further developed into an in-situ, sensitive and quantitative tool to study ferroelectric polymeric thin film structures.

Polymer materials are ubiquitous and play crucial roles in today's advanced technologies. Research on the development of polymers into new products such as drug delivery systems, engineered tissues, and energy harvesting/storage devices demonstrate that polymer technologies are needed to address many of the most critical challenges we face today in areas such as health care, informatics and renewable energy. In recent years, there has been great interest in highly functional polymeric systems ranging from synthesis and enabling fabrication to the development of novel and innovative characterization techniques. PVDF and its copolymers, as a family of highly functional polymer systems, have brought much renewed interest and excitement to the applied science community. This is due to their many appealing properties including light weight,

flexibility, mechanical toughness, chemical inertness, radiation hardness, optical transparency, high dielectric functions, and their ferro-, pyro-, and piezo- electricity. PVDF is chosen for this study because it is a unique ferroelectric polymer with realized and potential applications in energy harvesting, data storage and sensing.

It is well known that the final structures of polymeric systems are heavily dependent on the processing history and conditions. Depending on these processing conditions PVDF can have four possible crystalline phases; α-, γ-, δ-, and β-phase. The ferroelectric properties of PVDF thin films are the result of highly oriented β-phase crystalline domains within the amorphous matrix of the film.[70] When fabricated from the melt the most common crystalline phase of PVDF is the α-phase, and there are several post processing procedures that transitions the polymer from the α-phase to the β-phase in order to obtain a macroscopically ferroelectric film. The formation of the solid PVDF phases is very complex and often the final product contains a combination of amorphous and crystalline phases, therefore, it is very difficult to pin point how each individual molecular unit behaves.

It has also been shown very recently, that the understanding of the relaxation dynamics of PVDF with respect to temperature is still limited.[72] Sencadas *et al.*[72] have employed both dynamic mechanical and dielectric spectroscopic techniques to study the temperature dependence of semicrystalline PVDF. Two possible structural relaxation processes are proposed. One is called β-relaxation, which is assigned to cooperative segmental motions within the polymer chains in the amorphous regions of the film. The other is called $\alpha_c$-relaxation and corresponds to molecular motions within the crystalline portion of the polymer. However, the temperatures at which these relaxation processes occur are still not clearly understood.

Preparation and operating conditions of ferroelectric polymer systems involve a wide range of temperatures. Understanding the effects of temperature on molecular processes, in which structural relaxation dynamics play an essential role, is extremely important. Efforts are therefore made to exclusively identify these relaxation processes for the first time using SHG. The purpose of this research is to understand the structural formations and relaxation dynamics of polymeric systems by example of PVDF, while developing a sensitive and non-destructive nonlinear laser spectroscopic technique that will allow us to probe and interrogate these systems, providing valuable information for future science and technology.

SHG laser spectroscopy is a powerful technique which allows us to monitor molecular processes, such as crystalline phase transitions, dipole orientation and domain switching during and post production of the film. In order to obtain a comprehensive evaluation of the capability of SHG to structural relaxation dynamics of PVDF we first need to monitor the intensity of the SHG signal from samples with known phase and orientation, and then study the SHG response while modifying the phase/structure in a highly controlled manner. It is known that the intensity of the second harmonic photons has a quadratic dependence on the intensity of the fundamental light, the symmetry of the crystalline material and the presence of an electric field, as can be seen in equation 4.1:

$$I^{(2\omega)} = \left|\chi^{(2)} + \chi^{(3)}E(t)\right|^2 \left(I^{(\omega)}\right)^2 \qquad (4.1)$$

Where $I^{(2\omega)}$is the intensity of the second harmonic generated light, $\chi^{(2)}$ is the second order non-linear susceptibility, $\chi^{(3)}$ is the third order non-linear susceptibility, $E(t)$is the time dependent electric field, and $I^{(\omega)}$ is the intensity of the fundamental beam. The second order non-linear susceptibility occurs for crystal systems that lack inversion symmetry, or for regions in a material where there is a breakdown in center symmetry. [71] The β-phase of PVDF lacks inversion symmetry

and when aligned should be a strong source of second harmonic light, whereas the α-phase having center symmetry will generate no second harmonic light. Since there is no external applied electric field in these experiments and the intensity of the fundamental beam is constant, the only contribution to changes in the SHG intensity is the result of changes in the crystalline phase, orientation or structure.

**Sample Preparation**

The samples used in this study are cut from a commercially produced roll of semicrystalline PVDF film purchased from Measurement Specialties. The film is fabricated by a process known as extrusion in which the non-ferroelectric α-crystalline phase is originated from the melt. After extrusion, the film is uniaxially stretched at 80˚C to four times its original length resulting in the all-*trans* β-phase crystalline structure in which the chain axis of the polymer is parallel to the stretch direction and the film thickness is reduced to 9 μm. The thin film is then electrically poled in a direction along the surface normal of the film resulting in molecular dipoles in the β-phase crystal domains oriented in a direction parallel to the applied electric field. The finished product is a piezoelectric thin film.

Temperature dependent second harmonic studies are performed to observe the changes in SHG intensity as it correlates to transitions in domain orientation as well as crystalline phase. Two different sample sets are prepared in an attempt to decouple different materials relaxation and phase transition processes. One set is referred to as "un-clamped" since no restrictions are placed on these samples during the thermal annealing process. The other sample set has the outermost edges uniformly "clamped" during annealing to prevent the β-relaxation of the amorphous

polymer matrix by maintaining the stretched configuration of the polymer. For each sample set the PVDF is annealed for 30 minutes and then allowed to cool to room temperature. The temperatures used in this experiment were 50˚, 80˚, 100˚, 125˚, 150˚, 160˚, and 175˚C. All SHG measurements were taken at room temperature.

**Experimental Procedures**

A femtosecond laser used in this experiment is the Coherent Mira 900 which is tuned to a wavelength of 800 nm. The laser produces 150 fs pulses at a repetition rate of 76 MHz and pulse energy of ~10 nJ. The Mira is pumped by a stable Coherent 10 W Verdi diode-pumped 532 nm green laser. The average beam power of the Mira is reduced to 150 mW using a neutral density filter and is constantly monitored by a power meter. A red pass filter is used to remove the 532 nm light from the fundamental beam which is then focused to a spot of approximately 80 $\mu m^2$ area on the sample surface. The *p*-polarized second harmonic beam that is generated by the *p*-polarized fundamental beam is detected by a PMT and measured with a photon counter. A computer controlled motorized rotation stage provides the ability to change the angle to the surface normal while measuring the SHG signal. This is mounted on another rotation stage which allows the incident angle to be changed. The experimental setup is shown in figure 2 (b) where $\phi$ is the azimuthal angel and $\theta$ is the incident angle.

WAXS patterns are obtained by aligning the incident X-ray beam parallel to the normal direction, extrusion direction, or transverse direction of the film. The measurements were performed at 45 kV and 0.88 mA using a Confocal Max-Flux VR optic with a sealed tube microfocus X-ray source (Rigaku MicroMax-$002^+$), giving a highly focused beam of

monochromatic Cu Kα radiation (λ= 0.154 nm). The sample-to-detector distance was 140 mm, and the diffraction angle was calibrated using a $CaF_2$ standard. The patterns were collected using an image plate with 50 μm pixel size.

Transmission FTIR measurements were taken at normal incidence to the PVDF film using the Bruker Tensor 27 under Nitrogen atmosphere. 16 scans were co-added to obtain each IR spectrum in 400 – 1000 $cm^{-1}$ region with a 4 $cm^{-1}$ resolution.

**Experimental Results and Discussion**

Figure 4.1 shows the XRD pattern in the normal direction (a) and SHG results (b) of an as-received PVDF sample. The XRD pattern in figure 4.1 (a) provides the concentration of the crystalline phases of the PVDF. There is a well-defined peak located at 2θ = 20.26˚ which is characteristic of the β-phase, and the peaks located at 2θ = 17.66˚ and 26.56˚ are characteristic of the α-phase. These peaks indicate that the PVDF thin film consists mainly of the β-phase crystalline structure with a small percentage of α-phase.[73,74] Figure 4.1 (b) shows the second harmonic intensity as a function of azimuthal angle ϕ with a fixed incident angle of θ=45˚. At ϕ= 0˚ the orientation of the sample is such that the stretch direction of the PVDF is in parallel with the optical polarization of the incident beam, and at ϕ= 90˚ the stretch direction of the PVDF is perpendicular to the optical polarization of the incident beam. There are two main features that can be seen in this plot: large lobes present at ϕ=90˚ and 270˚, and two small lobes located at ϕ=0˚ and 180˚. These are explained by the high level of symmetry present in oriented β-phase PVDF thin film that has undergone uniaxial stretching and electrical poling.

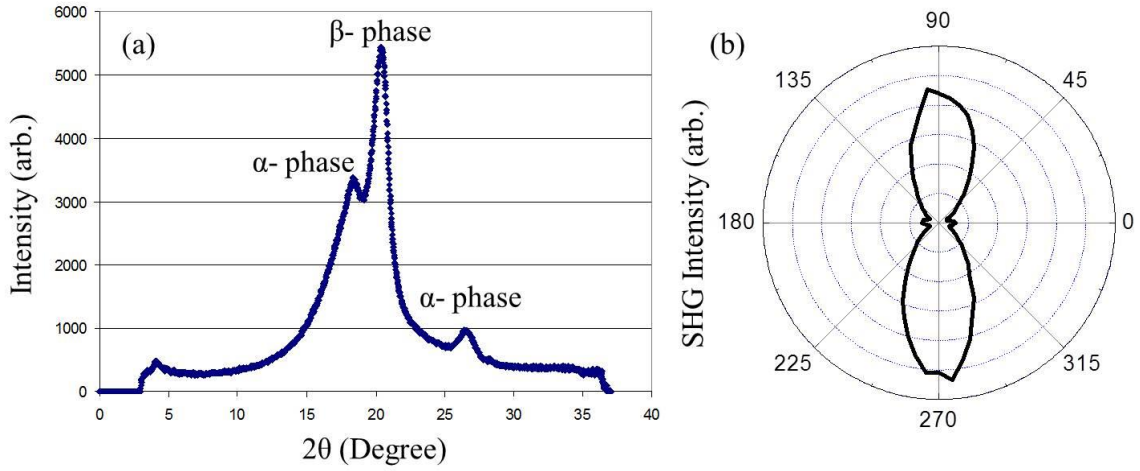


Figure 4.1: Optical and structure characterization of a uniaxially stretched, electrically oriented 9μm thick commercially produced β-phase PVDF thin film. (a) WXRD of the PVDF thin film in the surface normal direction. (b) Transmitted SHG intensity of the PVDF thin film rotated along the surface normal at a 45° incident angle.

Figure 4.2 shows the SHG intensity of an as received sample as a function of incident angle θ with two configurations in which the azimuthal angle ϕ is fixed. One configuration has the azimuthal angle fixed at ϕ=90˚ and the other fixed at the ϕ=0˚ position where the stretch direction of the film is perpendicular or parallel with the optical field, respectively. These positions are marked with the bold arrows in figure 4.2 (b). For both configurations the SHG intensity is at a minimum for normal incidence, θ=0˚. As the incident angle increases from the normal the SHG signal increases to a maximum position at approximately 40˚ followed by a decrease in intensity at incident angles beyond 40˚. The results in figure 4.2 are consistent with what is shown in figure 4.1 and confirm that the SHG signal is highly dependent on the azimuthal angle ϕ or the position of the carbon backbone chain axis with respect to the polarization of the optical field.

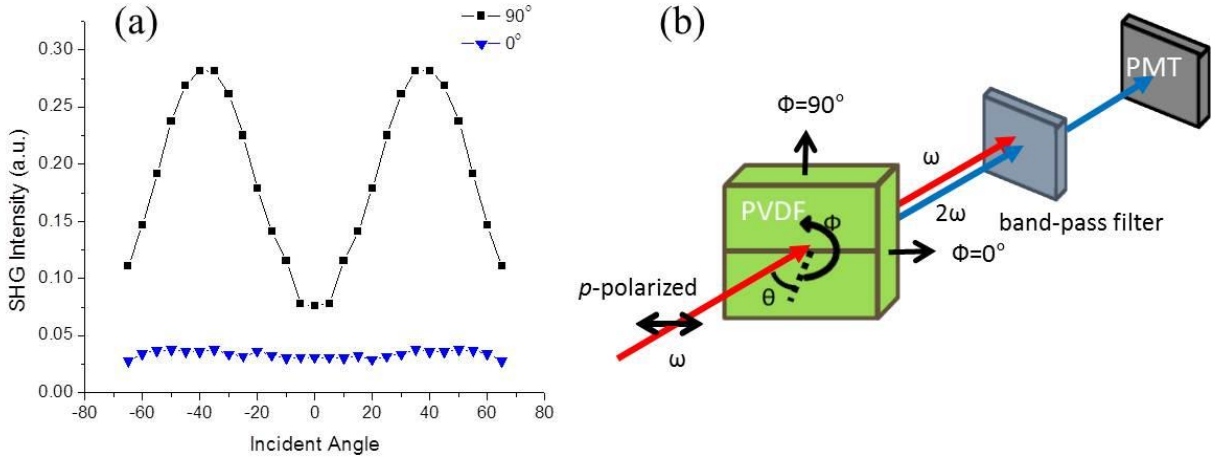


Figure 4.2: (a) SHG intensity change as a function of incident angle for the 9μm thick β-phase PVDF thin film. Φ= 0°, 90° indicates the stretch direction of the film is parallel, perpendicular to the E field component of the light respectively. (b) Experimental configuration for transmission SHG

Figure 4.3 shows the FTIR spectra (a) and SHG measurements (b) of the as received and annealed PVDF samples. The FTIR spectra in figure 4.3 (a) indicate that no crystalline phase change occurs to the PVDF samples due to annealing for temperatures below 175˚C with respect to the reference sample for both the un-clamped and the clamped sample set (FTIR spectra for the clamped sample set are not shown). The FTIR spectra of the sample annealed at 175˚C clearly shows an increase in the presence of α- phase PVDF as indicated by the increase in intensity of the peaks located at 532, 614, 764, 796 and 976 $cm^{-1}$. The reduction of the peak intensities located at 510 and 840 $cm^{-1}$ indicates a decrease in fraction of the β- phase PVDF in the film. The phase transition from β- to α- phase PVDF is also shown in figure 4.3 (c) where an azimuthal dependent SHG measurement of a sample annealed at 175˚C shows a complete loss of second harmonic symmetry.

Part (b) of figure 4.3 shows the intensity of the SHG signal as a function of annealing temperature for both the un-clamped and clamped PVDF sample sets. For the un-clamped samples

the SHG intensity dramatically decreases for annealing temperatures up to 80˚C and continues to decrease for subsequent heat treatments. The SHG intensity of the clamped samples remains somewhat constant for temperatures between 25˚ and 80˚C after which there is a drastic decrease in intensity. For both sample sets the rate of decrease in the SHG intensity levels off as the annealing temperatures from 100˚C approach the melting point at 175˚C.

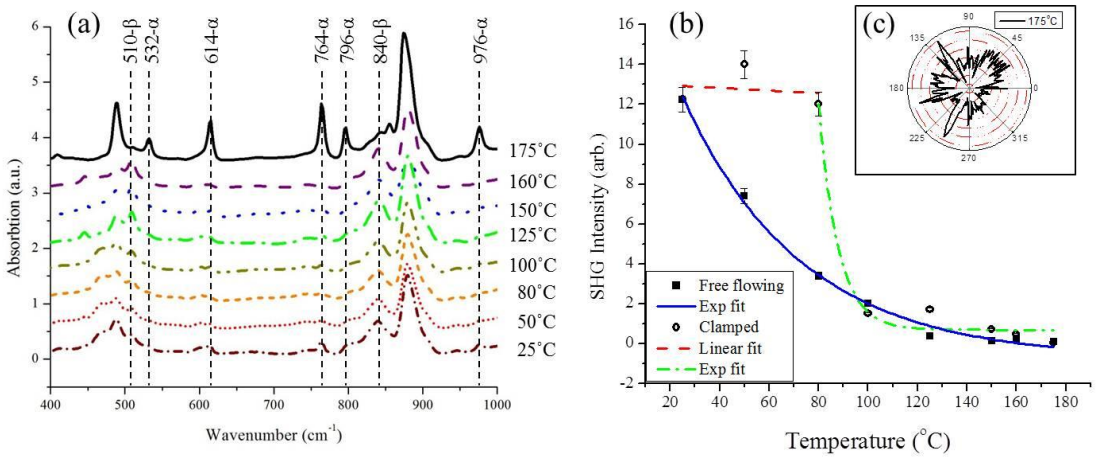


Figure 4.3: (a) FTIR spectra of as-received PVDF thin film and the films thermally annealed at elevated temperatures. Curves are offset and shifted upward for clarity (b) SHG intensity as a function of temperature. Insert, (c) is included to compare symmetry.

The different trends in SHG intensities for temperatures between 25˚ and 80˚C in each of the sample sets indicates that for the un-clamped samples the β-relaxation process is allowed whereas it is restricted for clamped sample set. β-relaxation occurs in the amorphous regions of the film resulting in a randomization of the crystalline domain orientation and a dramatic decrease in the SHG intensity. The $\alpha_c$-relaxation process appears in the crystalline regions of the PVDF and gives rise to randomization of the polymer chains and eventually the transition from β to α crystalline phase, as can be observed in the continued loss of SHG intensity at temperatures above 80˚C and loss of symmetry at 175˚C, respectively.

## Summary

In summary, the ability to acquire detailed information on the crystalline phase, domain orientations, and relaxation processes is essential for understanding the properties of ferroelectric polymer thin films such as PVDF. Spectroscopic techniques, such as WXRD and FTIR, provide information on the crystalline phase of semicrystalline polymers but are not sensitive to the domain orientations. By monitoring the SHG signal with respect to incident and azimuthal angles, we have shown that SHG is capable of not only providing details on the phase but is also sensitive to the orientation of the crystalline domains within a polymer thin film. We determined that the sensitivity of SHG to crystalline phase and orientation is due to the strong interactions between the molecular dipoles in the PVDF film and the optical field. We have also shown that SHG can be used as powerful yet sensitive, non-destructive and *in-situ* probe for observing changes in crystalline structure and orientation within polymer thin films which can lead to a better understanding of the relationship between temperature and relaxation dynamics within the film. With further development, SHG and electric field induced SHG (EFISH) will allow us to probe and better understand the ferroelectric properties of polymers such as PVDF, and to characterize more complex and confined polymer systems.

# CHAPTER V

## LINEAR AND NONLINEAR OPTICAL INVESTIGATION OF MULTILAYER PVDF/PC FILMS

### Introduction

It has been demonstrated by us and others that laser spectroscopy can be a very powerful tool to study polymeric systems in bulk and low dimensions, such as films and fibers.[75-79] The structure and the properties of polymers in general, such as PVDF and PC, can be highly dependent upon the fabrication processes involved. Thus, the structural, ferroelectric, piezoelectric, and thermal and electrical transport properties can be drastically modified or changed. As an example, nanofibers fabricated using the electrospinning process typically exhibit significant molecular orientation,[76,77] which could substantially alter their physical, chemical and optical properties. Indeed, recent studies of other highly oriented polymeric systems suggest that astonishingly high values of thermal conductivity, for example, are possible.[78,79] It is, therefore, very critical to initiate a systematic investigation of polymer systems from simple single layer structures to multilayers with a highly controlled and reproducible fabrication procedure.

Additionally, as discussed in previous chapters, PVDF and its copolymers represent a family of highly functional polymer systems. It has brought much renewed interest and excitement to the applied science community. On the other hand, it is known that PVDF can have four possible crystalline phases; α-, γ-, δ-, and β-phase. The piezoelectric properties of PVDF are the result of highly oriented β-phase crystalline domains within the amorphous matrix. Literature indicates when fabricated from the melt the most common crystalline phase of PVDF is the α-phase. There

is already an established library of post processing procedures to show how to convert PVDF from α-phase to β-phase in order to obtain a macroscopically ferroelectric material. It needs to be pointed out that the formation of the solid PVDF phases is very complex and often the final product contains a combination of amorphous and crystalline phases. It can be very difficult to pinpoint the structure, crystalline phase, and molecular orientation when PVDF and PC are fabricated via a co-extrusion technique and essentially stacked up into a multilayer polymer from the melt.

In this chapter SHG characterization of as-extruded and co-extruded single layer and multilayer PVDF and PC polymer films is performed. Confocal Raman laser spectroscopy is employed to obtain the structural information of individual layers and at the interface of a two layer PVDF/PC film. Conventional IR and XRD techniques are used to acquire the bulk information of the film and are then compared with the confocal Raman data to examine the structural and molecular information of the extruded polymer samples with respect to the bulk counterparts.

**Sample Preparation**

The samples used in this experiment are extruded polymer films fabricated by Case Western Reserve University. Single layer films of PVDF and PC are fabricated by extrusion and serve as control samples. Multilayer films of 2, 8 and 32 layers consisting of 50/50 PVDF/PC are fabricated using the forced assembly via micro layer co-extrusion technique. All films have an overall thickness of 12 μm with individual layer thicknesses of 6 μm, 1.5 μm, and 375 nm respectively. The samples are as-extruded from the melt which produces PVDF layers that have α crystalline phase.

**Experimental Procedures**

The SHG measurements are taken using a Coherent Mira 900 femtosecond laser which is pumped by a stable Coherent 10 W Verdi diode-pumped 532 nm green laser. The Mira is tuned to a wavelength of 800 nm, and produces 150 fs pulses with an energy of ~10 nJ per pulse at a repetition rate of 76 MHz. A neutral density filter is used to reduce the average beam power to 30 mW. The fundamental beam is then focused to a spot of approximately 50 $\mu m^2$ area on the sample surface. Figure 5.1 is the schematic of experimental setup. Figure 5.1 (a) is a simple layout of the experiments from the laser, to the sample to the detector. Figure 5.1 (b) is the front view along the light propagation direction, $\vec{k}$, with a horizontally polarized laser light, which is commonly defined as $\vec{p}$-polarization. The samples are mounted at a fixed incident angle of θ=45°as shown in figure 5.1 (c). Also, the extrusion direction of the sample is initially within the incident plane and so is the polarization of the laser beam. We defined the angle between the extrusion direction of the sample with respect to the incident plane as the azimuthal (Φ) and Φ = 0° at initial state as shown in figure 5.1 (b). The film is then rotated 360° along the azimuthal (Φ) using a computer controlled rotation stage. The second harmonic generated light (λ= 400 nm) is collected by a monochromater, detected by a PMT and measured with a photon counter.

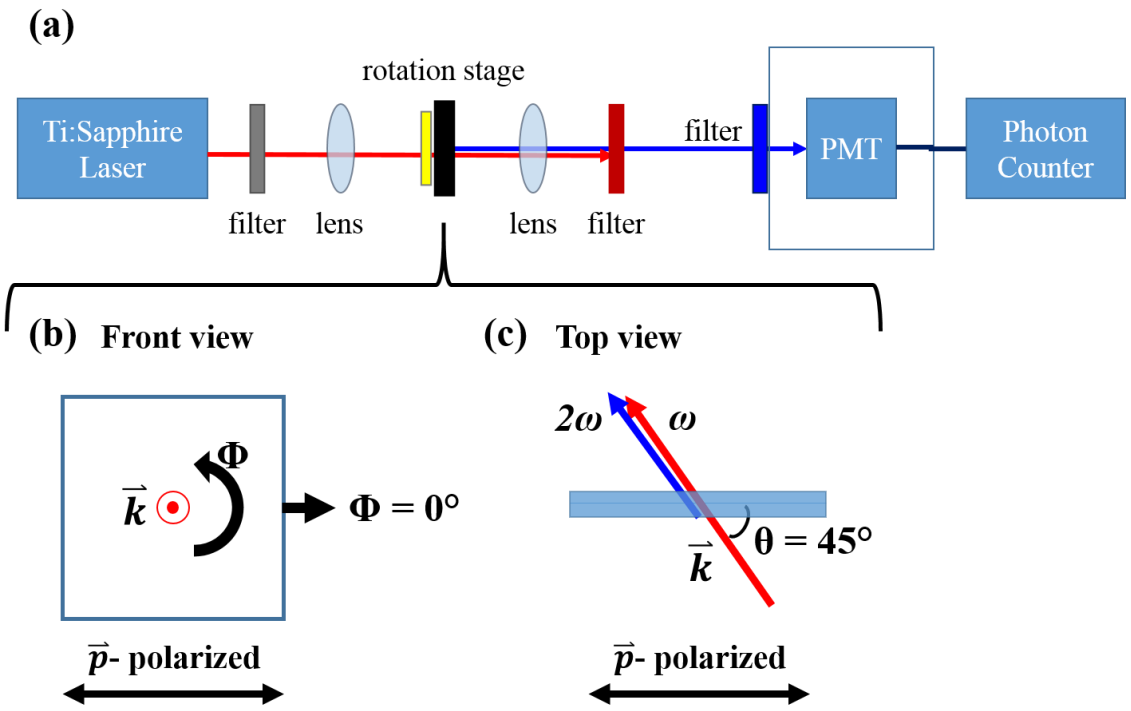


Figure 5.1: (a) Schematic of transmission SHG experimental setup. The plane of incidence is defined by $\vec{k}$ and $\vec{p}$ where (b) depicts a view of the surface of the sample at normal incidence and (c) is a view looking down at the plane of incidence in which the fundamental beam is at a 45° incident angle.

The Raman spectra are obtained using the confocal Raman capabilities of the Horiba micro-Raman system HR 800 and a 532 nm laser line which is focused to a spot size of approximately .70 $\mu m^2$ with a 100 x objective lens mounted on a piezoelectric stage. The piezo-driven stage is used for depth profiling measurements by moving the objective lens in the *z*-direction in 0.25 µm increments. At each step a spectrum ranging from 600-1050 wavenumbers is collected using a TE cooled (-70ºC) CCD array with a resolution of 0.5 $cm^{-1}$ while the sample is kept at room temperature.

Transmission FTIR measurements of the control and multilayer PVDF/PC films were taken at normal incidence to the films using the Bruker Tensor 27 under Nitrogen atmosphere.

Sixteen scans were co-added to obtain each IR spectrum in 400 – 4000 $cm^{-1}$ region with a 4 $cm^{-1}$ resolution.

WAXS patterns of the 50/50 PVDF/PC multilayer films are measured using a Confocal Max-Flux VR optic with a sealed tube microfocus X-ray source (Rigaku MicroMax-$002^{+}$) under 45 kV bias and 0.88 mA current. The incident X-ray beam is a highly focused beam of monochromatic CuKα radiation (λ=0.154 nm) that is aligned parallel to the normal direction, extrusion direction, or transverse direction of the films. The diffraction angle is calibrated using a $CaF_2$ standard, and the sample-to-detector distance is 140 mm. The X-ray diffraction patterns are collected using an image plate with a 50 μm pixel size.

**Experimental Results and Discussion**

Second harmonic generation measurements of single layer (a), 8 layer (b) and 32 layer (c) films as a function of azimuthal angle are shown in figure 4.2. Part (a) of figure 4.2 shows the SHG signal from the control single layer films of PVDF in black and PC in blue.

In previous work, the SHG intensities of highly oriented β-phase PVDF films were measured as a function of the azimuthal angle using a similar transmission experimental configuration as described in figure 5.1. When the orientation of the β-PVDF chain is parallel (ϕ = 0° and 180°) or perpendicular (ϕ = 90° and 270°) to the plane of incidence the SHG signal is at a minimum or maximum respectively. It was determined that the intensity of the SHG signal is dependent on the molecular dipole orientation with respect to the plane of incidence; the nonlinear polarization is at a maximum when the molecular dipoles are free to rotate along the carbon

backbone. This occurs when the polymer chain is perpendicular to the polarization of the incident beam.[75]

The extruded α-phase PVDF film has a strongly oriented SHG signal with maximum intensities at Φ= 90° and 270°. In α-phase PVDF a component of the molecular dipole moment is perpendicular to the chain axis and, similar to the β-phase PVDF, the nonlinear polarization is maximized as the dipoles rotate along the carbon backbone in response to the strong optical field. Also, the SHG signal is at a minimum when extruded direction of the polymer is parallel to the plane of incidence, at Φ= 0° and 180°. These results indicate that the α-PVDF polymer chains are oriented in the direction of extrusion. This is an important finding because the basic working principle of co-extrusion is based on the flow and spread of a polymer in its molten state. Clearly, the viscous flow and spread is not an isotropic process and results in molecular chains that are more aligned along co-extrusion direction.

The PC sample produces a SHG signal that is oriented with maximum intensities at Φ= 0° and 180°. It has been shown that, because of the dipolar aromatic character of the backbone, PC can exhibit nonlinear optical activity especially when the polymer chains are aligned in a preferential direction.[80] The benzene rings and oxygen that are present along the carbon backbone experience a strong nonlinear polarization between the delocalized electrons and the oxygen sites with high electron affinity. Therefore, just like the PVDF film, the PC polymer chains are also oriented in the direction of extrusion as indicated by the maximum SHG signal at Φ= 0° and 180°.

The multilayer films in figure 5.2 (b) and (c) have clearly displayed SHG signals of 4-fold symmetry with maximum intensities at Φ = 0°, 90°, 180°, and 270°. As expected due to the 50/50 PVDF/PC volume ratio, the SHG signals from the multilayer films have contributions from both the PVDF layers and the PC layers. The maximum SHG signals occur when the interaction

between nonlinear polarization and the optical field is strongest. This occurs when the dipoles are parallel to the polarization of the optical field. The dipoles in PVDF are perpendicular to the polymer chain whereas the dipoles in PC are parallel to the backbone. The 90° offset in the SHG maximums shows that both the PVDF and PC polymer chains are aligned along the direction of extrusion during the co-extrusion fabrication process.

The highly oriented SHG signal collected from the multilayer 50/50 PVDF/PC systems shown in figure 5.2 (b) and (c) demonstrate how sensitive and effective SHG is as a nondestructive technique for extracting information on the structure and orientation of PVDF and PC polymer chains within a multilayer system; which conventional Infrared, Raman, and XRD, for example, are unable to resolve.

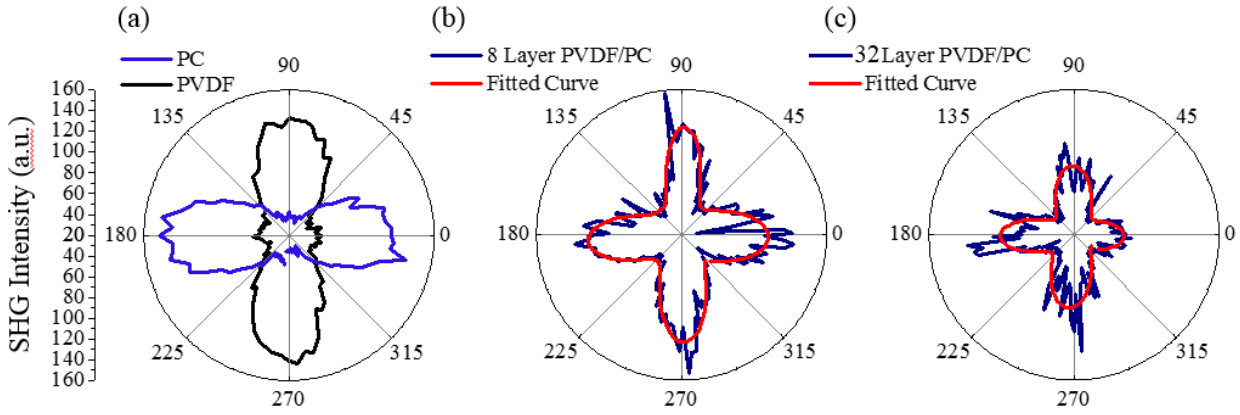


Figure 5.2: Transmission SHG measurements as a function of azimuthal angle of single layer PVDF and PC polymers (a), and 8 layer (b) and 32 layer (c) 50/50 PVDF/PC multilayer films.

Raman and Confocal Raman spectra of individual layers (a) and a two layer system (b) of PVDF and PC from a range of 600-650 wavenumbers are shown in figure 4.3. As can be seen in part (a) of figure 4.3 this spectral range is optimal because it has peaks located at 610 $cm^{-1}$ and 637 $cm^{-1}$ from the PVDF and PC films respectively that are similar in intensity and have no significant

overlap of Raman shifts, allowing clear observation of any changes in intensity of these peaks as a function of depth.

Confocal Raman spectra of a two layer PVDF/PC sample as a function of depth are shown in figure 5.3 (b). The different color spectra depict the different regions of the two layer system; where the PC layer is represented by the blue spectra, the PVDF layer is represented by the red spectra, and the yellow spectra show the interfacial region between the PVDF and PC layers. On the surface of the sample, at z = 0, the 610 $cm^{-1}$ PVDF peak is present and the intensity increases as function of depth until z is approximately 2.25 µm. In the region 2.5 µm < z < 3.25 µm both the 610 $cm^{-1}$ and 637 $cm^{-1}$ peaks are observed and have similar intensities indicating that this is the interfacial region consisting of both PVDF and PC. When z > 3.5 µm the 610 $cm^{-1}$ PVDF peak decreases significantly in intensity and the 637 $cm^{-1}$ PC peak intensity continues to increase until approximately 6 µm. After z = 6 µm the 637 $cm^{-1}$ PC peak intensity starts to decrease and continues to decrease until the bottom surface of the sample is exceeded.

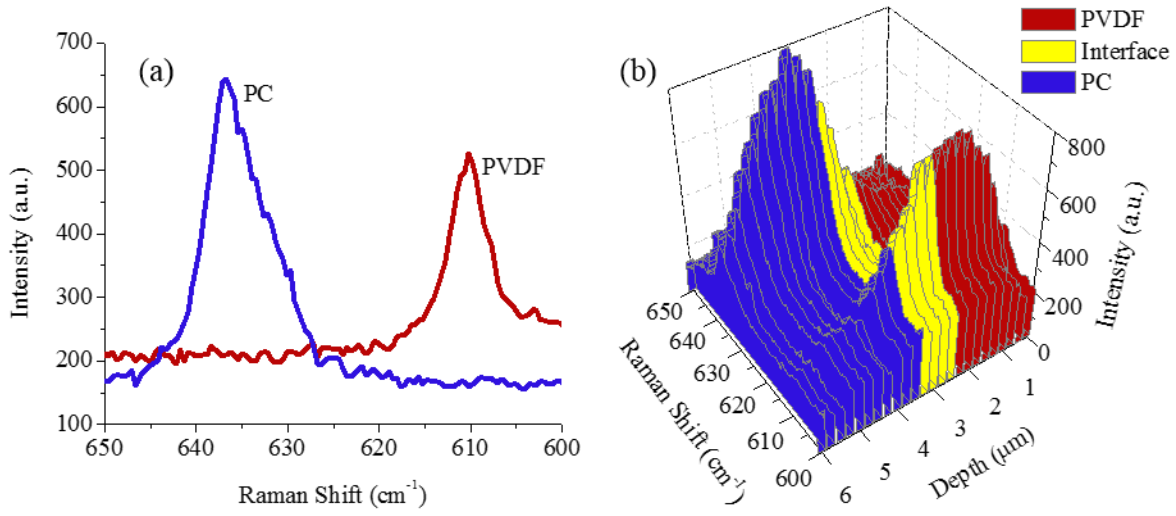


Figure 5.3: (a) Raman spectra of individual layers of PVDF and PC peeled from a two layer system. (b) Confocal Raman depth profiling spectra of a two layer 50/50 PVDF/PC system fabricated by co-extrusion.

These Raman spectra show that although the 2 layer film was fabricated under conditions that should result in a 12 μm film with 6 μm PVDF and PC individual layers, this film was 6 μm with PVDF and PC layers of approximately 3 μm in thickness. This inconsistency of film and layer thickness demonstrates a need for in-situ structural analysis of multilayer films produced via the co-extrusion process. The changes in intensity of the 610 $cm^{-1}$ PVDF and 637 $cm^{-1}$ PC Raman peaks shown in figure 5.3 (b) indicate that con-focal Raman microscopy is a powerful tool that can be used to study structural properties of the individual layers as well as the interfaces of multilayer polymer films with a lateral depth resolution of approximately 1 μm. This Raman information is important for developing an understanding of the properties of a multilayered polymer system especially within the individual layers and at the interface between layers.

FTIR spectra of control PVDF and PC films as well as a 2 layer 50/50 PVDF/PC multilayer film are shown in figure 5.4. The spectral regions of 400 to 1000 $cm^{-1}$ (a), 1000 to 2000 $cm^{-1}$ (b), and 2000 to 4000 $cm^{-1}$ (c) are shown separately for clarity purposes. Also, the spectral region in figure 5.4 (a) contains the identifying peaks that allow the crystalline phase of the PVDF film to be determined. Shown in figure 5.4 (d) are XRD spectra of 2 layer, 8 layer and 32 layer 50/50 PVDF/PC multilayer films. All spectra have been vertically offset for clarity.

In figure 5.4 (a), (b), and (c) the FTIR spectra of the PC control film is shown in blue, the PVDF control film is shown in red and the 2 layer film is in black. Comparison of the three spectra reveals that the IR absorbance peaks present in the PC and PVDF control films are also present in the FTIR spectra of the 2 layer film. The FTIR spectrum of the 2 layer 50/50 PVDF/PC film shows no additional absorbance peaks from that of the control films. This indicates that the interface between the two polymers is clean, meaning there is no strong intermolecular bonding or interactions between the PC and PVDF layers as a result of the co-extrusion fabrication process,

which may lead to characteristic absorption spectral changes. One may also infer there is no intermixing between PC and PVDF materials at interfacial region.

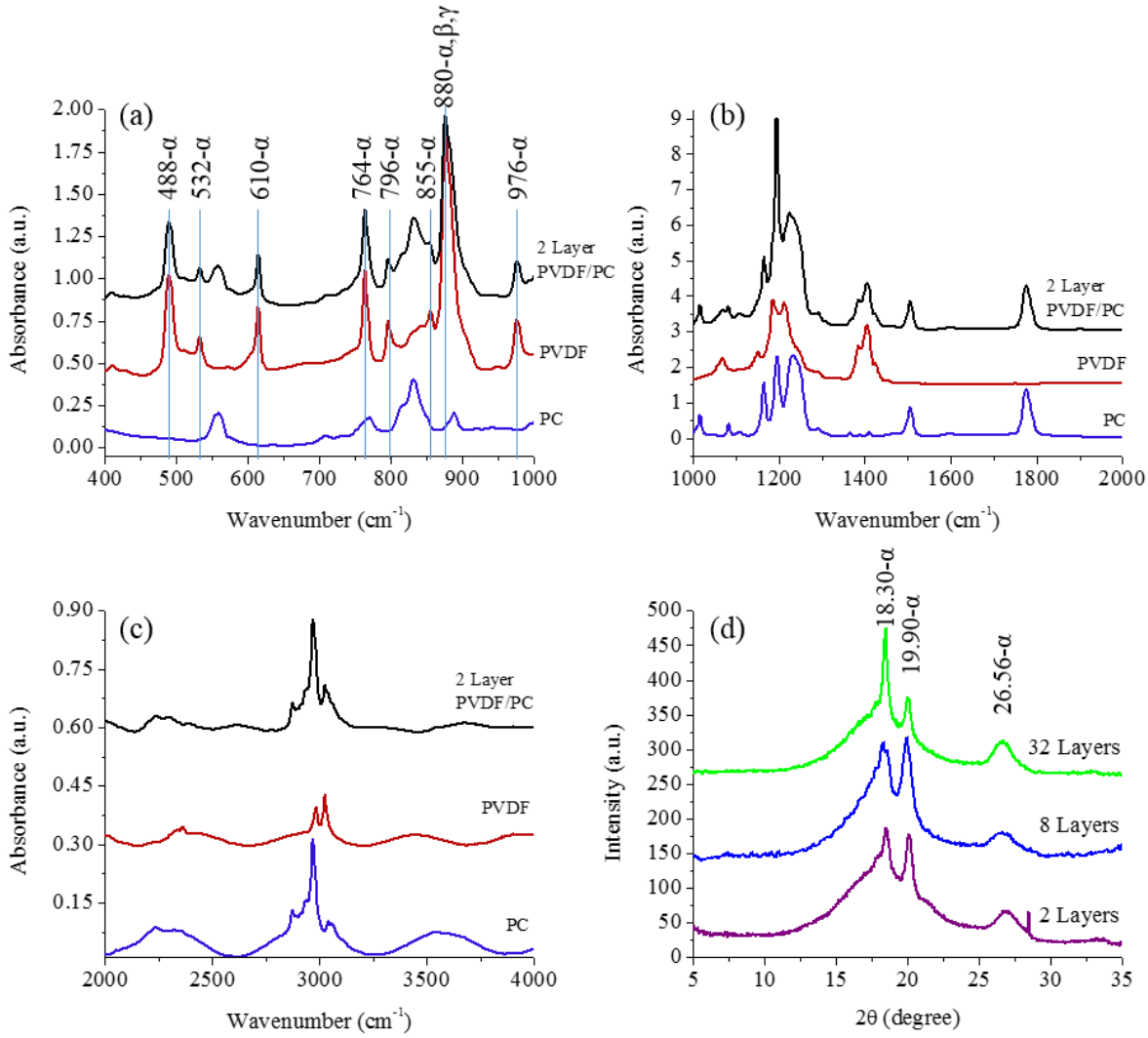


Figure 5.4: FTIR spectra (a), (b) and (c) of control PVDF and PC films, and 2 layer 50/50 PVDF/PC multilayer films. (d) XRD spectra of 2, 8, and 32 layer 50/50 PVDF/PC multilayer films. Spectra are vertically offset for clarity purposes.

The FTIR spectra for the PVDF film and the 2 layer 50/50 PVDF/PC film in figure 5.4 (a) have peaks located at 488, 532, 610, 764, 796, 855, and 976 $cm^{-1}$. These peaks identify the crystalline phase of the PVDF film as α-phase.[81] The peak located at 880 $cm^{-1}$ is common to all

phases of PVDF and is useful for identifying the polymer itself. The XRD spectra of the 2 layer, 8 layer and 32 layer 50/50 PVDF/PC multilayer films in figure 5.3 (d) have peaks located at 2θ= 18.30, 19.90, and 26.56° which also identifies the PVDF film as having the α crystalline phase.

**Summary**

In summary, it is important to monitor and understand the structural properties of polymer films fabricated via microlayer co-extrusion. It has been shown that SHG is a very effective and nondestructive technique for examining the molecular orientation of polymers during and after this fabrication process. Since the structure of these films can directly affect the dielectric and ferroelectric properties, what we can learn from SHG studies is valuable for technological breakthroughs in the development of polymer based capacitor and energy harvesting systems. While it makes lots of sense to use PVDF polymer with a high dielectric constant and layered with PC which has a high dielectric breakdown strength. Multilayer films consisting of 50/50 PVDF/PC by volume are fabricated via microlayer co-extrusion should boost capacitor's energy density. However, no contributions of molecular chain alignment has been considered to interpret a 3-fold increase in energy density of layered capacitor over the polymer blend.

Spectroscopic techniques such as XRD and FTIR are used to identify the phase of the PVDF films. Vibrational spectroscopic techniques such as FTIR and Raman provide information as to which polymers are present in a multilayer system, and it is determined that although PVDF and PC layers adhere well there is no strong molecular interactions between the two polymers. Confocal Raman provides structural information about the multilayer system as a function of depth with 1 μm depth resolution.

It is shown that by monitoring the SHG signal with respect to the azimuthal angle the orientation of the polymer chains of both PVDF and PC polymer films can be determined. The sensitivity of SHG to the chain orientation is due to the strong interactions between molecular dipoles in the polymer chains and the optical field. The dipoles in the PVDF polymer are oriented perpendicular to the chain axis and are parallel with the chain axis for the PC polymer. Keeping the optical field fixed and rotating the sample produces a SHG signal that has maximum intensities exactly 90° apart in the multilayer films, and when comparing the control PVDF and PC films. This shows that the polymer chains are oriented in the direction of extrusion during the co-extrusion fabrication process.

This evidence shows that SHG can be used as powerful yet sensitive, non-destructive and *in-situ* probe for observing the structure and orientation of polymer thin films which can lead to a better understanding of the dielectric and ferroelectric properties within the multilayer structure. With further development, SHG and electric field induced SHG (EFISH) will allow us to probe and better understand the ferroelectric and dielectric properties of polymers such as PVDF and PC, and to characterize more complex and confined polymer systems.

# CHAPTER VI

# EVALUATION AND IDENTIFICATION OF ELECTRODE MATERIALS FOR EFISH MEASUREMENTS OF PVDF THIN FILMS

## Introduction

Electric field induced second harmonic generation (EFISH) measurements can provide important information on the electric field distributions and the structural changes in multilayer PVDF/PC systems when under an applied potential. In order to perform EFISH measurements using the transmission experimental configuration it is essential to have transparent conducting electrodes. These films are extremely flexible and widely used materials such as ITO, which are very brittle, can fracture resulting in a non-uniform electric field. It is the focus of this chapter to explore alternate flexible transparent conducting materials to potentially replace ITO as electrodes for transmission EFISH measurements. Different materials are deposited on single layer PVDF films at variable thicknesses. UV-Vis transmission spectra are collected and electrical resistivity measurements are taken to determine which material will be used as transparent electrodes for future EFISH measurements.

## Transparent electrodes

Transparent conductive electrodes are essential components in many optoelectronic device such as ultraviolet (UV) photodiodes, LEDs, solar cells, touch panels, and infrared (IR) detectors. Over the years, metal oxides like indium tin oxide (ITO) have been widely used as transparent

electrodes in different technologies including organic light emitting diode, antistatic coating and EMI shielding. However, their uses have been limited due to lack of flexibility, brittleness, low binding strength, high production cost, and low infra-red transmittance.

Thin metal films have high transparency and flexibility, an easy and cheap production process and good electrical conductivity. They can potentially serve as good candidates to compete with the widely used transparent conductive electrodes, like ITO, for PVDF films and PVDF/PC multilayer systems. However, this effort does not eliminate the possibility of using ITO if other electrodes present technical problems.

**Experiment**

In this work efforts are made to replace transparent conductive oxides such as ITO. The main focus is to characterize the optical and electrical properties of ultra-thin metal films deposited on PVDF. Thin layers of metals, including nickel, aluminum, and molybdenum of different thickness (5 – 20 nm) are deposited on both sides of a 12 μm thick PVDF film using the Nano-Master NSC-3000 DC sputtering system. The transmittance is evaluated from 350 – 900 nm using the Hitachi 4000 spectrophotometer and electrical conductivity is measured using a 4-point probe system.

**Results and Discussion**

Figure 6.1 shows the UV-Vis transmittance results for different thicknesses of ITO (a), nickel (b), molybdenum (c), and aluminum (d) thin films deposited on a PVDF thin film. The

vertical lines are inserted to guide the eye at the fundamental and second harmonic generated wavelengths, 800 and 400 nm respectively. The three metal films have a much larger variance in transmittance with respect to thickness as compared to the ITO. For nickel films deposited on PVDF (b) the transmittance of both the 800 and 400 nm light is above 50% for the 5 nm thick film. The transmittance drops to less than 30% of 800 nm light and less than 20% of 400 nm light for 10 and 20 nm thick films. For the molybdenum thin films on PVDF (c) the transmittance of 800 nm is 75, 52, and 28% for 5, 10, and 20 nm thick films respectively, and the transmittance of 400 nm is 50, 26, and 10% for 5, 10 and 20 nm thick films respectively. The aluminum thin film on PVDF (d) has a transmittance of both 800 and 400 nm light that is above 75% for 5 nm thin films, above 50% for 10 nm films, but the transmittance drops below 50% for the 20 nm films. However, for all thicknesses of ITO on PVDF (a) the transmittance of the 800 nm light remained above 85%, and the transmittance of 400 nm light is more than 65%. The films that had the best transmittance of both the fundamental and second harmonic generated wavelengths are the 5, 10, and 20 nm ITO films and the 5 nm thick aluminum film.

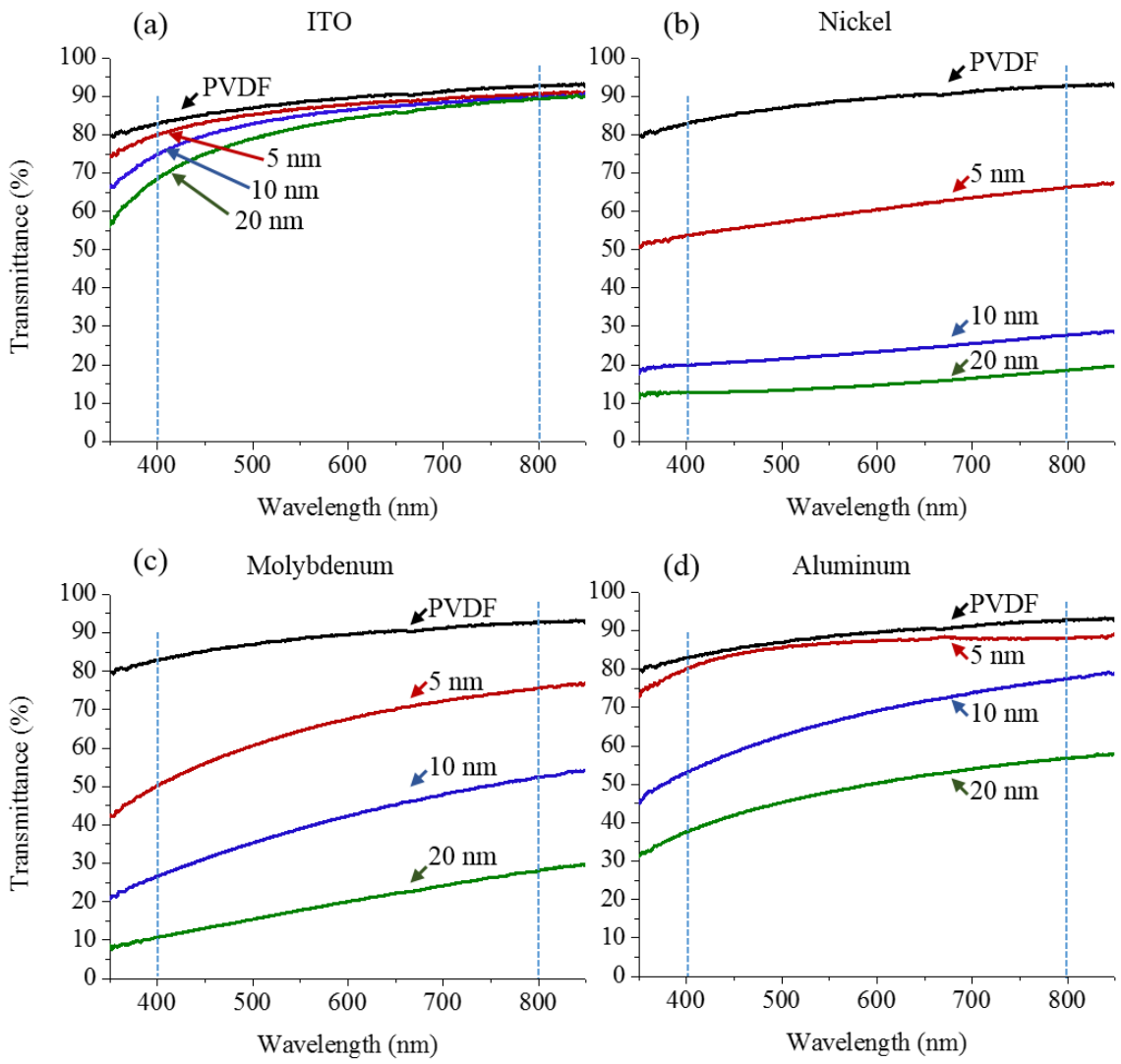


Figure 6.1: UV-Vis transmittance spectra of different thicknesses of (a) ITO, (b) Nickle, (c) Molybdenum, and (d) Aluminum deposited on both sides of a PVDF thin film.

Values for resistivity are collected using a four point probe and are shown in table 6.1 for each thickness of ITO, nickel, molybdenum, and aluminum. Results for the 5 nm ITO where not obtained and it is believed to be due to the brittleness of such a thin layer of the material. Data was also unable to be collected for the 5 nm aluminum. This may be due to the lack of continuity of the film. The high values of resistivity for 10 nm ITO and 10 nm molybdenum are thought to be the result of the probes cracking or possible puncturing the thin film. Overall, the 20 nm thin

films provided the best results which is more than likely due to film continuity and rigidity. However, the 20 nm aluminum film and the 10 nm nickel film gave the best value for resistivity. These results indicate that the 5 nm depositions are possibly too thin to provide uniform coverage and can be easily damaged. The thicker 20 nm films have better coverage, leading to a more uniform electric field distribution throughout the PVDF thin film.

Table 6.1: Resistivity values for different thicknesses of ITO, nickel, molybdenum, and aluminum thin films deposited on PVDF

| **Thickness / Material** | **5 nm** | **10 nm** | **20 nm** |
|---|---|---|---|
| **Indium Tin Oxide** | **N/A** | **32.82** | **1.858** |
| **Nickel** | **0.107** | **.0008** | **0.019** |
| **Molybdenum** | **.0378** | **190.6** | **.038** |
| **Aluminum** | **N/A** | **0.111** | **.0003** |

**Summary**

In summary, transparent conducting electrodes serve as an essential component to multilayer capacitor devices. In this research, transparent electrodes are essential for transmission EFISH measurements which will provide an understanding of structural changes and electric field distributions in multilayer PVDF/PC systems when under an applied field. Widely used materials like ITO tend to be brittle and fractures within the electrode film can result in non-uniform electric field.

To find an alternate flexible transparent electrode material; thin films of ITO, nickel, molybdenum, and aluminum are deposited onto PVDF in thicknesses of 5, 10 and 20 nm, and their optical and electrical properties were compared. Transmittance measurements of the films were taken using a UV-Vis spectrometer and the transmittance spectra of the fundamental and second harmonic generated light were analyzed for each material at each thickness. It is determined that the 5, 10, and 20 nm ITO and 5 nm aluminum films transmitted the most 800 and 400 nm light, transmitting between 65 to 85% of the light. Resistivity measurements indicated that thicker 20 nm electrodes provided more continuous coverage of the metal films on PVDF and that the thinner 5 nm were more prone to structural damage. The films that provided the least amount of resistivity were the 10 nm nickel and 20 nm aluminum indicating a continuous film, however these films had less than 50% transmittance of the 800 and 400 nm light. These results show that the best combination of transmittance and film continuity is that of the 20 nm ITO films.

# CHAPTER VII

# FUTURE WORK

## Introduction

In this chapter future work based on the knowledge gained from the results of the experiments in previous chapters is described. Combining and developing characterization techniques such as SHG, EFISH and Raman can provide a wealth of information about the structure and interface of a multilayer polymer systems. Three future research tasks are explained in detail and include; determining the depth resolution of confocal SHG and EFISH techniques, determining the dielectric breakdown strength of PVDF thin films, and performing confocal SHG, EFISH and Raman measurements on single and multilayer polymer systems. A detailed experimental approach in order to perform each task is described as well as the foreseeable challenges of each task.

## The significance of the materials and techniques

Non-centrosymmetric (NCS) PVDF and its co-polymers, when crystallized in β-phase, exhibit technologically important ferroelectric properties: piezoelectricity and pyroelectricity. It is evident that piezoelectric PVDF polymer has a distinct advantage over inorganic piezoelectric ceramic materials. It is flexible, light weight, optically transparent, cheap, is relatively easy to fabricate and can be produced in roll-to-roll. However, its major drawbacks include partial crystal

phase formation (50 – 70% crystalline phase), thermal stability, and durability. With multilayer systems, it is possible to use particular polymer(s) as the confining layer to stabilize the confined PVDF layers and even promote preferred crystalline phase and orientation. The success of the efforts will lead to technical breakthrough with enormous applications.

On the other hand, non-polar α-phase PVDF has played a critical role increasing the dielectric constant of materials for capacitor applications. To further boost the energy density of the capacitor, the materials must be able to withstand very high electrical fields, which leads to the problem of enhancing the dielectric breakdown of the materials. The ability to map out electric fields in materials along the anisotropic directions in great detail, such as the depth of multilayer systems, is extremely important.

Based on the research described in the previous chapters it has been successfully demonstrated that SHG and EFISH laser spectroscopy can indeed serve as a powerful diagnosis tool to provide basic information in a non-destructive and in-situ manner. Confocal Raman can serve as a complimentary and independent verification technique to EFISH and SHG.

To achieve both the material and technique significance stated above, the following tasks need to be performed.

**Future research tasks**

*TASK 1: Determination of the Depth Resolution of SHG* $\left(\chi^{(2)}\right)$ *and EFISH* $\left(E * \chi^{(3)}\right)$ *Laser Spectroscopy with and without Confocal Options*

The confocal Raman investigation of a multilayer PVDF/PC system has demonstrated a submicron depth resolution with a piezo-controlled sample stage. Although the current custom-

made SHG and EFISH experimental set ups are expected to have an even better spatial resolution of hundreds of nanometers, efforts will be made to use PVDF-TrFE/PET multilayer systems with different layer thickness in order to determine the spatial resolution experimentally. It is known that, because of the greater portion of fluorine atoms, PVDF- TrFE conforms to the β-crystalline phase[1], and this remains true even as the co-polymer is layered in a multilayer film. The existence of the β-phase results in a strong signal in both the non-confocal SHG and XRD measurements, but the α-phase of PVDF and the PET polymer provide little to no SHG signal. Because of the extreme differences in SHG intensity, the PVDF-TrFE/PET co-extruded multilayer system can be used to obtain the SHG depth resolution.

***Approach:*** At least 4 sets of PVDF- TrFE//PET multilayer samples will be fabricated from Prof Zhu's group at CWRU with each layer having a thickness of 200, 500, 1000, and 5000 nm. With the help of a piezo-stage, the obtained SHG signal should reflect the thickness of PVDF-TrFE layer. A good quality Gaussian beam approximation and model fitting will lead to a good estimate of spatial resolution. The spatial resolution obtained from SHG measurements will be further verified with the confocal Raman technique as described in Chapter 5.

***Foreseeable Challenges:*** *1)* PVDF-TrFE/PET samples may have a relatively weak SHG signal as a result of the isotropic crystal domain orientation. Thermal annealing and 1D or 2D mechanical stretching of the film can be used produce a highly oriented PVDF-TrFE film which will enhance the SHG signal and improve the measurements (see Table 3.1 in Chapter 3). *2)* Extra caution may be needed to evaluate potential photothermal degradation/damage of the sample to be studied.

*TASK 2: Confocal SHG $\left(\chi^{(2)}\right)$, EFISH $\left(E * \chi^{(3)}\right)$ and Raman Measurements of Single Layered PVDF Film from Case Western Reserve University*

It is known that PVDF fabricated through co-extrusion from the melt conforms to the α-crystalline phase. However, there has been no research conducted in literature describing what happens when an external electric field is applied to the film; for example, whether a possible electrical field induced phase transition occurs. No study has reported if the α-phase under very high external electrical field can lead to permanent structure formation different from the parent α-phase. In order to perform this task one must address the immediate issue of dielectric breakdown so that EFISH experiments can be conducted.

*Determining dielectric breakdown*

In order to prevent a number of unnecessary repetitions of complicated and time consuming experiments with ultrafast laser systems, it is important to obtain information about the dielectric breakdown prior to the SHG, EFISH, and Raman measurements. Knowing the dielectric breakdown threshold for particular electrodes used is important.

***Approach:*** After electrode deposition, as described in Chapter 5, the films will be tested with a dielectric testing platform equipped with a Keithley function generator providing the input signal and a precision high voltage generator from Trek which can produce voltages up to ±4 KV. Since a typical thin film to be studied in the current research is a few tens of microns the field strength can be tested up to $\pm 10^8$ V/m. The same high voltage system will also be used for EFISH and Raman measurements.

***Foreseeable Challenges:*** Electrical contacts may not be trivial when the deposited electrodes have weak binding with the substrate. Caution must be exercised to ensure a good contact and that voltage is applied uniformly throughout the electrode surface. Multi-testing points may be exercised.

*SHG, EFISH and Raman measurements of single layer films*

The primary objectives of combining SHG, EFISH and Raman techniques are to learn how the materials respond before, during and after the application of an external electrical field. SHG and Raman measurements should provide an understanding of how the applied electrical field can modify the structure of the film either transiently or permanently. Information about the internal electric field can be extracted from the results obtained from the EFISH experiments when the basic parameters are known. It is then possible to map the electric field inside the layers spatially and at interfaces in multilayer systems. The success of this kind of 3D mapping will have great value to many applications ranging from devices, sensors, to systems. Certainly, it will help to illustrate/understand the dielectric breakdown, which is significant for capacitor applications.

***Approach:*** Due to the fact that the detected SHG signal from a sample consists of both SHG $\left(\chi^{(2)}\right)$ and EFISH $\left(\mathrm{E} * \chi^{(3)}\right)$ when electrical field is applied, only SHG $\left(\chi^{(2)}\right)$ can be obtained when the local electric field E is zero. Likewise, the pure EFISH signal can only be collected for materials with zero $\chi^{(2)}$ as discussed in the previous sections. In order to decouple the SHG and EFISH, a square waveform input signal will be used for high voltage generator with an incremental amplitude increase after each cycle, as shown in figure 7.1. In a general sense, when a voltage is applied to the system, SHG signal collected should contains two contributions SHG $\left(\chi^{(2)}\right)$ and

EFISH $\left(E * \chi^{(3)}\right)$. When the voltage is zero after time $t_0$, the measured SHG signal should only be SHG $\left(\chi^{(2)}\right)$ by definition. The change of the later is the result of applied electrical field leading to the symmetry breakdown of the material. Raman, on the other hand can also shed light on the structural changes during the times when the voltage is zero and non-zero.

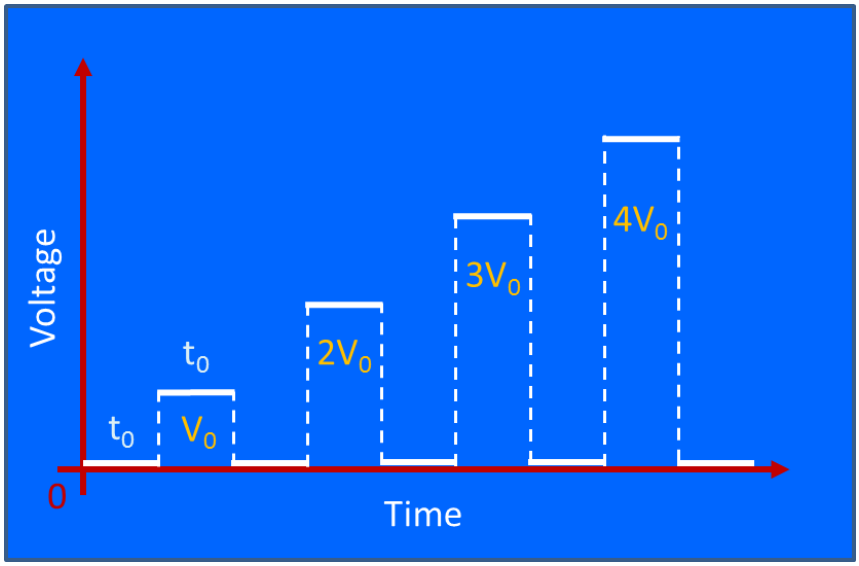

Figure 7.1: Schematic of proposed EFISH experiment

With the combination of these three techniques and the method of applying the external electrical field, rich and detailed information related to the material's response in terms of structural change and internal electrical field can be obtained. A linear fitting of the square root of total SHG signal versus the applied electric field shown below may be used for low field regime, which will allow us to obtain the two constants *a* and *b*.

$$\sqrt{I^{2\omega}} = |a + bE(0)| \qquad (7.1)$$

At high fields, nonlinear modeling may be expected and sophisticated modeling may be applied.

***Foreseeable Challenges:*** This is a very critical step of this research. It is not only the time to lead to new discovery but also to lay the solid foundation for multilayer study. Here is a list of anticipated challenges and problems: 1) Experimental set-up is challenging due to the limited space – optical microscope, high voltage connections, delicate samples and electrical isolation; 2) photon induced dielectric breakdown far below the value of dielectric breakdown without photoexcitation, and 3) weak SHG signals that make the measurements more challenging.

*TASK 3: Confocal SHG* $\left(\chi^{(2)}\right)$*, EFISH* $\left(E * \chi^{(3)}\right)$ *and Raman Investigation of Multilayered PVDF/PC Systems*

With the basic knowledge of what has been accomplished and summarized in previous chapters, previous sections and Tasks 1 and 2, this task is the highlight of this research. Much has already been learned from the studies of single and multilayer systems, and what is new will be the integration of the methods for information gathering. From a materials aspect this research can provide the basic information required to change and modify the rules for material design after knowing, for example, why and how the dielectric breakdown occurs in multilayer system for capacitors. If the micro- and nano-confinement effects will or will not alter the materials physical and chemical properties. And how to change and/or modify the properties as desired. From a characterization approach, new methodology has been developed to characterize layered systems which have applications for energy storage, sensors and devices, such as, OLED, OPV and PVDF based sensors so long as a good optical window exists.

***Approach:*** In order to extract meaningful and reliable information on interfacial polarization, ion (charged impurity species), the electrical field within each polymer layer and the

electrical field at the interface, a set of PVDF/PC multilayer films will be made. Two critical sample parameters will be used in combination of information obtained in Task 1&2. They are number of layers and layer thickness. The plan in this research may be limited to systems with under 32 layers and layer thickness will range from tens of nanometers to tens of micrometers. The samples will be fabricated at CWRU using Prof. Zhu and Baer's co-extrusion facility. The lower thickness limit is based on the instrumental limitations beyond which no meaningful information may be obtained. The upper limit is a layer thickness which is much larger than Rayleigh range of the laser spectroscopy and the system can be treated as bulk materials (negligible interfacial and physical confinement effects on the layer under investigation). Sample preparation, data collection, procedures and cautions will be similar to those in Task 2.

So far, all of the current and future research described in this dissertation is experimental in nature. The combination of the SHG, EFISH and Raman techniques will provide a deep understanding of the multilayer system. Also, because the sample sets are carefully planned in terms of number of layers and layer thicknesses, a multilayered film consisting of *n* ferroelectric and non-ferroelectric layers can be viewed as films connected in series along the thickness direction in an alternating manner. The constitutive equation of the *i*th layer may be written as: $D_i = \varepsilon_i E_i + P_i$, where *i* is an integer between 1 and *n*. *D*, ε, *E*, and *P* represent the dielectric displacement, permittivity, electric field, and ferroelectric polarization, respectively. $P_i$ generally depends on $E_i$ in a complicated manner and a model for describing *P–E* relations must be used. When the layer, say *j*th layer, is non-ferroelectric, then $P_j$ is set to zero.

***Foreseeable Challenges:*** Confocal SHG $\left(\chi^{(2)}\right)$ and EFISH $\left(\mathrm{E} * \chi^{(3)}\right)$ and Raman can be very sensitive, non-destructive, non-contact, and *in-situ* techniques that can provide a wealth of information on structure and interfaces of a multilayer polymer system. However, these

techniques do have some limitations: 1) photoinduced material damage due to the high peak power of ultrafast laser; 2) material handling issues may cause delamination, and 3) a realistic interfacial polarization model development.

**Summary**

In summary, three future research tasks are explained in detail along with a detailed experimental approach to perform each task and the foreseeable challenges of each. The first task involves determining the depth resolution of confocal SHG and EFISH techniques using PVDF-TrFE/PET multilayer systems with varying layer thicknesses. The second is determining the dielectric breakdown strength and performing confocal SHG, EFISH and Raman measurements on single layer α-phase PVDF films. And finally taking SHG, EFISH and Raman measurements of multilayer PVDF/PC polymer systems that have variable thicknesses.

Combining characterization techniques such as SHG, EFISH and Raman can provide a wealth of information about the structure and interface of a multilayer polymer systems. Developing these techniques further using confocal methods can allow three dimension mapping of the electric field distributions, and how the application of these electric fields effect the structure of individual polymer layers and the interfaces between polymers. The information provided by these characterization methods is critical if these multilayer polymer systems are to be integrated in current technology.

# CHAPTER VIII

## SUMMARY

Due to the fact that the co-extrusion technology is enabling and novel, this area of research is relatively open and much can be explored. From the materials characterization perspective, linear and non-linear confocal spectroscopy can address a number of important and critical issues which include: Second harmonic generation laser spectroscopy (SHG) to study PVDF films; confocal Raman spectroscopy to study PVDF containing multilayered dielectric films layer-by-layer with sub-micron spatial resolution; and SHG laser spectroscopy to investigate multilayer PVDF/PC co-extruded films from overall film measurements then into individual layers. Also, the development of the confocal electric field induced second harmonic (EFISH) technique will allow mapping of the local electric field inside the multilayer film when an external high voltage is applied or device interfaces or junctions where the local electrical field is not zero. The results and fundamental understanding of the materials systems will provide valuable guidance for better design principles of polymer multilayer films and device optimization.

The ability to acquire detailed information on the crystalline phase, domain orientations, and relaxation processes is essential for understanding the properties of ferroelectric polymer thin films such as PVDF. Spectroscopic techniques, such as WXRD and FTIR, provide information on the crystalline phase of semicrystalline polymers but are not sensitive to the domain orientations. By monitoring the SHG signal with respect to incident and azimuthal angles, we have shown that SHG is capable of not only providing details on the phase but is also sensitive to the orientation of the crystalline domains within a polymer thin film. We determined that the sensitivity of SHG to

crystalline phase and orientation is due to the strong interactions between the molecular dipoles in the PVDF film and the optical field. We have also shown that SHG can be used as powerful yet sensitive, non-destructive and *in-situ* probe for observing changes in crystalline structure and orientation within polymer thin films which can lead to a better understanding of the relationship between temperature and relaxation dynamics within the film.

It is also important to monitor and understand the structural properties of polymer films fabricated via microlayer co-extrusion. It has been shown that SHG is a very effective and nondestructive technique for examining the molecular orientation of polymers during and after this fabrication process. Since the structure of these films can directly affect the dielectric and ferroelectric properties, what we can learn from SHG studies is valuable for technological breakthroughs in the development of polymer based capacitor and energy harvesting systems. While it makes lots of sense to use PVDF polymer with a high dielectric constant and layered with PC which has a high dielectric breakdown strength. Multilayer films consisting of 50/50 PVDF/PC by volume are fabricated via microlayer co-extrusion should boost capacitor's energy density. However, no contributions of molecular chain alignment have been considered to interpret a 3-fold increase in energy density of layered capacitor over the polymer blend.

Spectroscopic techniques such as XRD and FTIR are used to identify the phases of the PVDF films. Vibrational spectroscopic techniques such as FTIR and Raman provide information as to which polymers are present in a multilayer system, and it is determined that although PVDF and PC layers adhere well. However, there is no strong molecular interactions between the two polymers which result in vibrational frequency shifting, linewidth broadening or new bands appears due to molecular structure and selection rules change. Confocal Raman used provides

structural information about the multilayer system as a function of depth with 1 μm depth resolution or better.

It is shown that by monitoring the SHG signal with respect to the azimuthal angle the orientation of the polymer chains of both PVDF and PC polymer films can be determined. The sensitivity of SHG to the chain orientation is due to the interactions between molecular dipoles in the polymer chains and the optical field. A strong 2$^{nd}$ nonlinear susceptibility $\chi^{(2)}$ is observed from the dipoles in the PVDF polymer that are oriented perpendicular to the chain axis and are parallel along the chain axis for the PC polymer. Keeping the optical field fixed and rotating the sample produces a SHG signal that has maximum intensities exactly 90° apart in the multilayer films, and when comparing the control PVDF and PC films. This shows that the polymer chains are oriented in the direction of extrusion during the co-extrusion fabrication process.

This evidence shows that SHG can be used as powerful yet sensitive, non-destructive and *in-situ* probe for observing the structure and orientation of polymer thin films which can lead to a better understanding of the dielectric and ferroelectric properties within the multilayer structure. With further development, SHG and electric field induced SHG (EFISH) will allow us to probe and better understand the ferroelectric and dielectric properties of polymers such as PVDF and PC, and to characterize more complex and confined polymer systems.

Another clear advantage and can be extremely useful, though not involved in current dissertation is the fact that this technique is insensitive to the surroundings or environments, such as in liquids, gases, vacuum or even embedded in solids, as long as they are optically transparent.

## REFERENCES

### Chapter 1:


1. Andrew J. Lovinger, "Ferroelectric Polymers," *Science* **220**, 1115-1121 (1983).

2. R. G. Kepler and R. A. Anderson, "Ferroelectricity in polyvinylidene fluoride," *J. Appl. Phys.* **49**, 1232 (1978).

3. J. B. Lando and W. W. Doll, "The polymorphism of poly(vinylidene fluoride). I. The effect of head-to-head structure," *J. Macromol. Sci. Phys.* **B2**, 205-218 (1968).

4. M. Mackey, A. Hiltner, E. Baer, L. Flandin, M. A. Wolak, and J. A. Shirk, "Enhanced Breakdown Strength of Multilayered Films Fabricated by Forced Assembly Microlayer Coextrusion"*, J. Phys. D: Appl. Phys.***42**, 175304 (2009).

5. M. Ma, K. Vijayan, A. Hiltner, and E. Baer, "Thickness Effects in Microlayer Composites of Polycarbonate and Poly(styrene-acrylonitrile)," *Journal of Materials Science*, **25**, 2039-2046 (1990).

6. T. Kazmierczak, H. Song, A. Hiltner, and E. Baer, "Polymeric One-Dimensional Photonic Crystals by Continuous Coextrusion," *Macromol. Rapid Commun*. **28**, 2210-2216 (2007).

7. Y. Jin, H. Tai, A. Hiltner, E. Baer, and J. S. Shirk, "New Class of Bioinspired Lenses with a Gradient Refractive Index," *Journal of Applied Polymer Science*. **103**, 1834-1841 (2007).

8. H. Wang, J. K. Keum, A. Hiltner, E. Baer, B. Freeman, A. Rozanski, and A. Galeski, "Confined Crystallization of Polyethylene Oxide in Nanolayer Assemblies," *Science*. **323**, 5915 (2009).

9. M. A. Wolak, M. J. Pan, A. Wan, J. S. Shirk, M. Mackey, A. Hiltner, E. Baer, and L. Flandin, "Dielectric Response of Structured Multilayered Polymer Films Fabricated by Forced Assembly," *Appl. Phys. Lett*,**92**, 113301 (2008).

10. A. Flores, C. Arribas, F. Fauth, D. Khariwala, A. Hiltner, E. Baer, F. J. Balta-Calleja, and F. Ania, "Finite Size Effects in Multilayered Polymer Systems: Development of PET Lamellae Under Physical Confinement," *Polymer*. **51**, 4530-4539 (2010).

11. Y. D. Glinka, N. H. Tolk, and J. K. Furdyna, "Time-Resolved Second Harmonic Generation Study of Buried Semiconductor Heterointerfaces using Soliton-Induced Transparency*," Appl. Phys. Lett.* **91**, 231104 (2007).

12. H. Park, J. Qi, Y. Xu, G. Lüpke, and N. Tolk, "Polarizataion-Dependent Temporal Behaviour of Second Harmonic Generation in Si/SiO2 Systems," *Journal of Optics* **13**, 055202 (2011).

13. White Y. V., Lu X, Pasternak R., Tolk N. H., Chatterjee A., Schrimpf R. D., Fleetwood D. M., Ueda A., Mu R., "Studies of Charge Carrier Trapping and Recombination Processes in Si/SiO2/MgO Structures Using Second-Harmonic Generation," *Applied Physics Letters*. **88** (2006).

14. Boyd, R.W., *Nonlinear Optics*. 1992, Boston: Academic Press.

15. Haojiang, D. and Weiqiu, C., *Three Dimensional Problems of Piezoelasticity.* 2001, New York, Nova Science Publishers, Inc.

**16.** K. M. Ok, E. O. Chi, and P. S. Halasyamani, "Bulk Characterization Methods for Non-Centrosymmetric Materials; Second-Harmonic Generation, Piezoelectricity, Pyroelectricity, and Ferroelectricity," *Chem. Soc. Rev*. **35**, 710-717 (2006).

17. V. V. Kochervinski "Structural Changes in Ferroelectric Polymers Under the Action of Strong Electric Fields by the Example of Polyvinylidene Fluoride," *Crystallography Reports.* **51**, 88-107 (2006).

**Chapter 2:**

18. T. H. Maiman, "Stimulated Optical Radiation in Ruby," *Nature* **187**, 493 (1960).

19. P. A. Franken et. al., "Generation of Optical Harmonics," *Physical Review Letters* **7**, 118 (1961).

20. H. Kawai, "The Piezoelectricity of Poly(vinylidene Fluoride)," *Jpn J. Appl. Phys* **8**, 975 (1969).

21. J. G. Bergman Jr., J. H. McFee, and G.R. Crane, "Pyroelectricity and Optical Second Harmonic Generation in Polyvinylidene Fluoride Films," *Appl. Phys. Lett.* **18**, 203 (1971).

22. R. G. Kepler and R. A. Anderson, "Ferroelectricity in polyvinylidene fluoride," *J. Appl. Phys.* **49**, 1232 (1978).

23. G. T. Boyd, "Optical Second-Harmonic Generation as an Orientational Probe in Poled Polymers," *Thin Solid Films* **152**, 295 (1987).

24. S. Bauer, "Second Harmonic Generation of Light in Ferroelectric Polymer Films with a Spatially Nonuniform Distribution of Polarization," *IEEE Trans. on Electrical Insulation* **27**, 4 (1992).

25. S. Bauer, G. E. Eisenmenger, W. Eisenmenger, and H. Schlaich, "Second Harmonic Generation with Partially Poled Polymers," *Optics Letters* **18**, 1 (1993).

26. S. Bauer, "Poled Polymers for Sensors and Photonics Applications," *J. of Appl. Phys.* **80**, 10 (1996).

27. A. Kubono, T. Kitoh, K. Kajikawa, S. Umemoto, T. Tekezoe, A. Fukuda, and N. Okui, "Second Harmonic Generation in Poly(vinylidene Fluoride) Films Prepared by Vapor Deposition Under an Electric Field," *Jpn. J. Appl. Phys.* **31**, 8B (1992).

28. O. A. Aktsipetrov, T. V. Misuryaev, T. V. Murzina, S. P. Palto, N. N. Petukhova, V. M. Fridkin, Y. G. Fokin, and S. G. Yudin, "Two-dimensional Ferroelectricity and Phase Transitions in PVDF Langmuir-Blodgett Films Probed by Second Harmonic Generation," *Integrated Ferroelectrics* **35**, 1-4 (2001).

29. N. Tsutsumi, Y. Ueda, T. Kiyotsukuri, A. S. Dereggi, and G. T. Davis, "Thermal Stability of Internal Electric Field and Polarization Distribution in Blend of Polyvinylidene Fluoride and Polymethylmethacrylate," *J. Appl. Phys.* **74**, 5 (1993).

30. A. Wicker, B. Berge, J. Lajzerowicz, and J. F. Legrand, "Nonlinear Optical Investigation of the Bulk Ferroelectric Polarization in a Vinylidene Fluoride/Trifluoroethylene Copolymer," *J. Appl. Phys.* **66**, 1 (1989).

31. K. A. Verkhovskaya, A. D. Grishina, N. I. Kuznetsova, L. Y. Pereshivko, T. V. Krivenko, and V. V. Savel'ev, "Second Harmonic Generation in Vinylidene Fluoride-Trifluoroethylene Copolymers Doped with Donor-Acceptor Molecules," *Crystallography Reports* **47**, 2 (2002).

32. J. Y. Chang, M. Domnner, C. Chang, and L. W. Lin, "Piezoelectric Nanofibers for Energy Scavenging Applications," *NanoEnergy* **1**, 3 (2012).

33. L. Zhu, Q. Wang, "Novel ferroelectric polymers for high energy density and low loss dielectrics," *Macromolecules* **2012**, *45*, 2937-2954.

34. M. Mackey, A. Hiltner, E. Baer, L. Flandin, M. A. Wolak, and J. S. Shirk, "Enhanced breakdown strength of multilayered films fabricated by forced assembly microlayer coextrusion," *J. Phys. D: Appl. Phys.* **2009**, *42*, 175304.

35. F. Kremer, and A. Schönhals, *Broadband Dielectric Spectroscopy*. Springer: Berlin; NewYork, 2003; p xxi, 729 p.

36. M. Mackey, D. E. Schuele, L. Zhu, L. Flandin, M. A. Wolak, J. S. Shirk, A. Hiltner, and E. Baer, "Reduction of dielectric hysteresis in multilayered films via nanoconfinement," *Macromolecules* **2012**, *45*, 1954-1962.

37. H. Wang, J. K. Keum, A. Hiltner, and E. Baer, "Confined crystallization of PEO in nanolayered films impacting structure and oxygen permeability," *Macromolecules* **2009**, *42*, 7055-7066.

38. H. Wang, J. K. Keum, A. Hiltner, E. Baer, B. Freeman, A. Rozanski, and A. Galeski, "Confined crystallization of polyethylene oxide in nanolayer assemblies," *Science* **2009**, *323*, 757-760.

39. M. Sandrock, M. Wiggins, J. S. Shirk, H. W. Tai, A. Ranade, E. Baer, and A. Hiltner, "A widely tunable refractive index in a nanolayered photonic material," *Appl. Phys. Lett.* **2004**, *84*, 3621-3623.

40. Y. Jin, H. Tai, A. Hiltner, E. Baer, and J. S. Shirk, "New class of bioinspired lenses with a gradient refractive index," *J. Appl. Polym. Sci.* **2007**, *103*, 1834-1841.

41. G. Beadie, J. S. Shirk, A. Rosenberg, P. A. Lane, E. Fleet, A. R. Kamdar, Y. Jin, M. Ponting, T. Kazmierczak, Y. Yang, A. Hiltner, and E. Baer, "Optical properties of a bio- inspired gradient refractive index polymer lens," *Opt Express* **2008**, *16*, 11540-11547.

42. G. Beadie, M. L. Sandrock, M. J. Wiggins, R. S. Lepkowicz, J. S. Shirk, M. Ponting, Y. Yang, T. Kazmierczak, A. Hiltner, and E. Baer, "Tunable polymer lens," *Opt Express* **2008**, *16*, 11847-11857.

43. H. M. Song, K. Singer, J. Lott, Y. H. Wu, J. F. Zhou, J. Andrews, E. Baer, A. Hiltner, and C. Weder, "Continuous melt processing of all-polymer distributed feedback lasers," *J. Mater. Chem.* **2009**, *19*, 7520-7524.

44. Y. H. Wu, K. D. Singer, R. G. Petschek, H. Song, E. Baer, and A. Hiltner, "Mode delocalization in 1D photonic crystal lasers," *Opt Express* **2009**, *17*, 18038-18043.

45. G. L. Mao, J. Andrews, M. Crescimanno, K. D. Singer, E. Baer, A. Hiltner, H. M. Song, and B. Shakya, "Co-extruded mechanically tunable multilayer elastomer laser," *Opt Mater Express* **2011**, *1*, 108-114.

46. J. Lott, C. Ryan, B. Valle, J. R. Johnson, D. A. Schiraldi, J. Shan, K.D. Singer, and C. Weder, "Two-photon 3D optical data storage via aggregate switching of excimer-forming dyes," *Adv. Mater.* **2011**, *23*, 2425-2429.

47. M. A. Wolak, M. J. Pan, A. Wan, J. S. Shirk, M. Mackey, A. Hiltner, E. Baer, and L. Flandin, "Dielectric response of structured multilayered polymer films fabricated by forced assembly," *Appl. Phys. Lett.* **2008**, *92*, 113301.

48. M. A. Wolak, A. S. Wan, J. S. Shirk, M. Mackey, A. Hiltner, and E. Baer, "Imaging the effect of dielectric breakdown in a multilayered polymer film," *J. Appl. Polym. Sci.* **2012**, *123*,2548-2557.

49. M. Mackey, D. E. Schuele, L. Zhu, and E. Baer, "Layer confinement effect on charge migration in polycarbonate/poly(vinylidene fluorid-*co*-hexafluoropropylene) multilayered films," *J. Appl. Phys.* **2012**, *111*, 113702.

50. Z. Zhou, M. Mackey, J. Carr, L. Zhu, L. Flandin, and E. Baer, "Multilayered polycarbonate/poly(vinylidene fluoride-*co*-hexafluoropropylene) for high energy density capacitors with enhanced lifetime," *J. Polym. Sci., Part B: Polym. Phys.* **2012**, *50*, 993-1003.

51. E. Baer, A. Hiltner, J. S. Shirk, and M. A. Wolak, "Multilayer polymer dielectric film," US 20100172066, 20100708, 2010.

52. M. Lallart, *Ferroelectrics - Characterization and Modeling*. InTech: Online, 2011.

53. K.A. Cook-Chennault, N. Thambi, and A.M. Sastry, "Powering MEMS portable devices – a review of non-regeneraive and regenerative power supply systems with special emphasis on piezoelectric energy harvesting systems," *Smart Mater. Struct*. **2008**, 17 43001.

54. Y. Liu, G. Tian, Y. Wang, J. Lin, Q. Zhang and H.F. Hofmann, "Active piezoelectric energy harvesting: general principle and experimental demonstration," *J Intelligent Mater Systems and Strutures*, **2009**, 20, 575.

55. R. Guigon, J. Chaillout, T. Hager and G. Despesse, "Harvesting raindrop energy: experimental study," *Smart Mater Struct*, **2008**, 17, 15039.

56. F. Guan, J. Pan, J. Wang, Q. Wang and L. Zhu, "Crystal orientation effect on electric energy storage in poly(vinyldene fluoride-co-hexafluoropropylene)copolymers," *Macromolecules*, **2010**, 43, 384-392.

57. Y. Fu, E.C. Harvey, M.K. Ghantasala and G.M. Spinks, "Design, fabrication and testing of piezoelectric polymer PVDF microactuators," *Smart Mater Struct*, **2006**, 15, S141-146.

58. M. Mackey, A. Hiltner, E. Bear, L. Flandin, M. A. Wolak, and J. A. Shirk, "Enhanced breakdown strength of multilayered films fabricated by forced assembly microlayer coextrusion," *J. Phys. D: Appl. Phys*. **2009**, 42, 175304.

59. K.I. Winey and R. Vaia, "Polymer Nanocomposites," *MRS Bulletin*, **2007**, 32, 314.

60. K.I. Winey, T. Kashiwagi and M. Mu, "Improving electrical conductivity and thermal properties of polymers by the addition of carbon nanotubes as fillers," *MRS Bulletin*, **2007**, 32, 348.

61. V.V. Kochervinskii, "Ferroelectricity of polymers based on vinylidene fluoride," *Russian Chemical Reviews*, **1999**, 68, 821-857.

62. R.D. Simons, M.A. Rodriguez-Perez, J.A. De Saja, C.J.L. Constantino, "Tailoring the structural properties of PVDF and P(VDF-TrFE) by using natural polymers as additives," *Polymer Engineering and Science*, **2009**, 49, 2150-2157.

**Chapter 3:**

63. T. H. Maiman, "Stimulated optical radiation in ruby," *Nature* **187**, 493 (1960).

64. L. F. Johnson, R. E. Dietz, and H. J. Guggenheim, "Optical maser oscillation from $Ni^{2+}$ in $MgF_2$ involving simultaneous emission of phonons," *Phys. Rev. Lett.* **11**, 318 (1963).

65. P. P. Sorokin and J. R. Lankard, "Stimulated Emission Observed from an Organic Dye, Chloro-Aluminum Phthalocyanine," *IBM J. Res. Dev.* **10**, 162 (1966).

66. F.P. Schafer, W. Schmidt, and J. Volze, "Organic Dye Solution Laser," *App. Phys. Lett.* **9**, 306 (1966).

67. J. C. Walling, H. P. Jenssen, R. C. Morris, E.W. O'Dell, and O. G. Pererson, "Tunable-Laser Performance in BeAlz04:$Cr^{3+}$," *Opt. Lett.* **4**, 182 (1979).

68. K. F. Wall and A. Sanchez, "Titanium Sapphire Lasers," *The Lincoln Laboratory Journal* **3**, 447 (1990).

**Chapter 4:**

69. M. Mackey, A. Hiltner, E. Baer, L. Flandin, M. A. Wolak, and J. S. Shirk, "Enhanced breakdown strength of multilayered films fabricated by forced assembly microlayer coextrusion," *J. Phys. D: Appl. Phys.*, **42,** 175304 (2009).

70. Andrew J. Lovinger, "Ferroelectric Polymers," *Science* **220**, 1115-1121 (1983).

71. R. W. Boyd, *Nonlinear Optics* (Academic Press, Boston, 1992) p.44.

72. V. Sencadas, S. Lanceros-Méndez, R. Sabater i Serra, A. Andrio Balado, and J.L. Gómez Ribelles, "Relaxation dynamics of poly(vinylidene fluoride) studied by dynamical mechanical measurements and dielectric spectroscopy," *Eur. Phys. J. E*, **35**, 41 (2012).

73. L. Yu and P. Cebe, "Effect of nanoclay on relaxation of poly(vinylidene fluoride) nanocomposites," *J. Poly. Sci. Part B: Polym Phys*, **47**, 2520 (2009).

74. R. Gregorio, Jr.,"Determination of the α, β, and γ crystalline phases of poly(vinylidene fluoride) films prepared at different conditions," *Appl Polym. Sci*. **100**, 3272 (2006).

**Chapter 5:**

75. J Jones, L Zhu, N Tolk, and R Mu, "Investigation of ferroelectric properties and structural relaxation dynamics of polyvinylidene fluoride thin film via second harmonic generation", *Applied Physics Letters*. **103**, 07290 (2013).

76. L. M. Bellan and H. G. Craighead, "Molecular orientation in individual electrospun nanofibers measured via polarized Raman spectroscopy," Polymer, vol. 49, no. 13–14, pp. 3125–3129, Jun. 2008.

77. M. Richard-Lacroix and C. Pellerin, “Orientation and Structure of Single Electrospun Nanofibers of Poly(ethylene terephthalate) by Confocal Raman Spectroscopy,” Macromolecules, vol. 45, no. 4, pp. 1946–1953, Feb. 2012.

78. S. Shen, A. Henry, J. Tong, R. Zheng, and G. Chen, “Polyethylene nanofibres with very high thermal conductivities,” Nat. Nanotechnol., vol. 5, no. 4, pp. 251–255, Mar. 2010.

79. X. Huang, G. Liu, and X. Wang, “New Secrets of Spider Silk: Exceptionally High Thermal Conductivity and Its Abnormal Change under Stretching,” Adv. Mater., vol. 24, no. 11, pp. 1482–1486, Mar. 2012.

80. R J Gulotty, C A Langhoff, and S E Bales, “Nonlinear optical activity of bisphenol A polycarbonate and related polymers,” *SPIE Nonlinear Optical Properties of Organic Materials III* **1337**, 258-270 (1990).

81. R. Gregorio, Jr.,”Determination of the α, β, and γ crystalline phases of poly(vinylidene fluoride) films prepared at different conditions,” *Appl Polym. Sci*. **100**, 3272 (2006).

82. L. Yang, X, Li, E., Allahyarov, P.L. Taylor, Q.M. Zhang, and L. Zhu, “Novel polymer ferroelectric behavior via crystal isomorphism and the nanoconfinement effect,” *Polymer* **2013**, 54, 1709-1728.

83. M. Mackey, D. E. Schuele, L. Zhu, L. Flandin, M. A. Wolak, J. S. Shirk, A. Hiltner, and E. Baer, “Reduction of dielectric hysteresis in multilayered films via nanoconfinement,” *Macromolecules* **2012**, *45*, 1954-1962.

84. Andrew J. Lovinger, “Ferroelectric Polymers,” *Science* **220**, 1115-1121 (1983).